catalysts

MDPI

Review

Boosting the Characterization of Heterogeneous Catalysts for H_2O_2 Direct Synthesis by Infrared Spectroscopy

Maela Manzoli

Department of Drug Science and Technology, University of Turin, Via Pietro Giuria 9, 10125 Turin, Italy; maela.manzoli@unito.it; Tel.: +39-011-670-6663

Received: 30 November 2018; Accepted: 19 December 2018; Published: 2 January 2019

Abstract: Infrared (IR) spectroscopy is among the most powerful spectroscopic techniques available for the morphological and physico-chemical characterization of catalytic systems, since it provides information on (i) the surface sites at an atomic level, (ii) the nature and structure of the surface or adsorbed species, as well as (iii) the strength of the chemical bonds and (iv) the reaction mechanism. In this review, an overview of the main contributions that have been determined, starting from IR absorption spectroscopy studies of catalytic systems for H_2O_2 direct synthesis, is given. Which kind of information can be extracted from IR data? IR spectroscopy detects the vibrational transitions induced in a material by interaction with an electromagnetic field in the IR range. To be IR active, a change in the dipole moment of the species must occur, according to well-defined selection rules. The discussion will be focused on the advancing research in the use of probe molecules to identify (and possibly, quantify) specific catalytic sites. The experiments that will be presented and discussed have been carried out mainly in the mid-IR frequency range, between approximately 700 and 4000 cm^{-1}, in which most of the molecular vibrations absorb light. Some challenging possibilities of utilizing IR spectroscopy for future characterization have also been envisaged.

Keywords: H_2O_2 direct synthesis; IR spectroscopy; FTIR characterization; Diffuse Reflectance Fourier Transform IR characterization; catalyst characterization; Pd catalysts; AuPd catalysts; bimetallic catalysts

1. The Direct Synthesis of Hydrogen Peroxide from Molecular Hydrogen and Oxygen

Hydrogen peroxide is a benign and environmentally friendly oxidising reagent extensively employed in the production of both fine and bulk chemicals. Moreover, it finds application in water treatment, paper and pulp bleaching, textiles, and in large-scale selective oxidation processes, such as the epoxidation of olefins, the hydroxylation of aromatics, and the synthesis of cyclohexanone oxime, which is strategic for nylon-6 production (Figure 1) [1]. These applications would greatly benefit from on-site, moderate-scale production facilities in order to reduce transport costs. However, H_2O_2 is produced worldwide on a multi-million ton scale annually by the energy intensive Riedl−Pfleiderer anthraquinone oxidation process [2]. Significant amounts of organic waste due to the anthraquinone, along with several energy consuming separation and concentration steps, and the use of benzene as the solvent are the main drawbacks of the process, which is economically feasible only in large-scale plants. In this frame, the research is devoted to the development of new economic scalable methods for the direct synthesis of H_2O_2 starting from hydrogen and oxygen and to the optimization of efficient oxidation catalysts able to work in the presence of H_2O_2 for sustainable production.

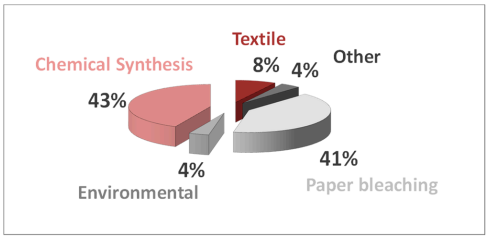

Figure 1. Main applications of H_2O_2.

The direct synthesis reaction can be considered as a dream reaction involving molecular H_2 and O_2, in which the formation of H_2O_2 takes place upon proton−electron transfer to O_2 and *OOH intermediates. Conversely, the formation of H_2O implies the O–O bond cleavage of the surface *OOH species [3]. As a matter of fact, H_2O_2 selectivity is ruled by the competitive O–H bond formation and O–O bond cleavage.

H_2O_2 direct synthesis can potentially halve the cost with respect to the anthraquinone commercial process, resulting in a much lower environmental impact, also due to the possibility to avoid chlorine for oxidation chemistry [1,4]. In addition, the direct synthesis reaction has the potential to produce inexpensive H_2O_2 at the mid-scale in geographically distributed facilities, because such facilities would have much lower capital and operating costs than Riedl-Pfleiderer plants with comparable dimension [5,6]. Nevertheless, no alternative process for H_2O_2 direct synthesis has yet been marketed, despite several published patents [2,7–11] and literature papers [10,12–25]. Indeed, selectivity is still far from being high and must be significantly improved for a successful industrial exploitation. Indeed, water is the most thermodynamically favoured product (as shown in Figure 2) and the H_2-O_2 gas mixtures are explosive in a very broad range of compositions (4–96%), posing severe limitations to the practicability of the process under safe conditions.

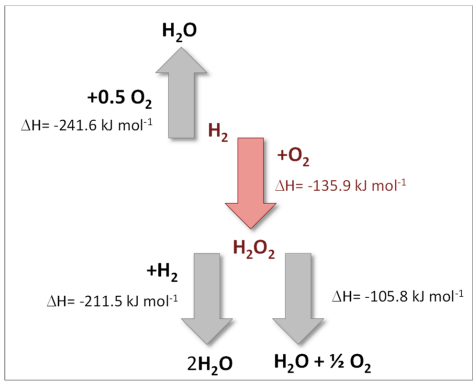

Figure 2. Reactions involved in the direct synthesis of H_2O_2.

Palladium, either alone [26–37] or associated with gold [17,22,25,38–44], with platinum [45–48], with tin [49,50], with nickel [51], with tellurium [52], and with zinc [53,54], has been extensively studied and it is considered as the best catalyst in terms of both activity and selectivity, the latter being fundamental for commercial applications [19,55]. Rh and Ru additives have detrimental effects on the H_2O_2 yields because they promote H_2O_2 decomposition and/or enhance H_2 to H_2O activity [19].

The effect of the nature of the support (ZrO_2, Ga_2O_3, CeO_2, SiO_2, ThO_2, CeO_2–ZrO_2, Al_2O_3, carbon etc.) on the catalytic activity and selectivity was extensively investigated [19,32,56]. Carbon porosity and surface structure play a key role to achieve high chemoselectivity [38].

Unluckily, the catalysts employed to perform the direct synthesis of H_2O_2 are also active for its decomposition. It was shown that an acid pretreatment of the carbon support of AuPd alloy catalysts turned off the H_2O_2 decomposition [21]. In particular, the acid treatment induced a decrease in the size of the bimetallic nanoparticles, which were supposed to decorate the sites, hence inhibiting the

decomposition reaction, and hydrogen selectivity >95% were achieved. It was also demonstrated that H_2O_2 can be produced over metallic Pd sites which have been geometrically and electronically modified by additives, such as Cl^-, Br^-, oxygen, and/or nitrogen atoms of the support [21,57–59].

In this frame, it has also been shown that the modification with ligands of Pd nanoparticles supported on carbon created a hybrid nanostructure with unique catalytic performance [60].

Acids and halides have been commonly added in order to improve the H_2O_2 selectivity [1,12,58,61,62]. Indeed, acid additives are able to impede the H_2O_2 decomposition, whereas halide additives hinder water formation [1,14,61]. Nevertheless, both corrosion of the reactor and dissolution of the catalytically-active metal occur in the presence of acid additives. Alternative acid supports, such as solid acid supports like SO_3H- functionalized mesoporous silicas [24], SO_4^{2-}-, Cl^--, F^--, and Br^--doped zirconia [63], insoluble heteropolyacids [64–66], and insoluble heteropolyacids supported mesoporous silica [66,67], cesium-containing $CsH_3-PW_{12}O_{40}$/MCF [68,69], and have been reported to act as acid sources. Cs-exchanged phosphotungstic acid was employed as an acid additive to an Au-Pd/TiO_2 catalyst with significant improvement of the H_2O_2 synthesis rate and selectivity with respect to the promotional effect of common oxides and non-halo acids [70].

It has also been reported that acidity of the catalysts played a crucial role in determining the catalytic performance in the direct synthesis of hydrogen peroxide [66,67]. Approaches, such as the catalyst wet pre-treatment method (CWPM), involving the post-modification of commercially available Pd catalysts with aqueous solutions of Br^- with different concentrations, have been shown to enhance the selectivity [30].

2. Infrared Absorption Spectroscopy as a Tool for Catalyst Characterization

Infrared (IR) absorption spectroscopy is one of the most popular characterization tools to describe heterogeneous catalysts [71]. In FTIR analysis, a molecule is excited to a higher vibrational energy state upon absorption of the IR radiation. Only the molecules that undergo to a variation of the dipole moment during the vibrational transition are IR active [72]. It should be, therefore, remembered that both O_2 and H_2 molecules, i.e., the reactants involved in the direct synthesis of hydrogen peroxide, owing to their symmetry, are IR inactive (no change of the dipole moment).

The energy associated to the excited states is related to the molecular bond vibrations, such as stretching, bending, rocking, twisting, wagging, as well as out-of-plane deformations, which take place at different frequencies or wavenumbers (cm^{-1}) in the IR spectroscopic region [72]. The position of a band is defined by Equation (1), which describes the behaviour of an anharmonic oscillator:

$$\nu = 1/2\pi c \cdot (k/\mu)^{1/2} \quad (1)$$

where ν is the frequency, c is the light speed, k is the force constant related to the bond between the two atoms which constitute the oscillator, and μ represents the reduced mass of the oscillator. As a consequence, the position of an IR band depends either on the strength of the bond or on the mass (isomeric effect). This implies that the specific physicochemical properties of the molecule or adsorbate (i.e., when performing a FTIR experiment of adsorbed probe molecules), i.e., the bonds involved and the local environment, affect the position of the IR absorbance peak, making the technique diagnostic, since the corresponding IR spectrum represents a fingerprint of that particular functional group, such as C–H, O–H, C=O, C≡O, N=N, and so on. Moreover, similar vibrational modes possess similar energetics, meaning that the interpretation of the IR spectra of unknown species is useful to identify the specific moieties that constitute the sample. In particular, the position of the absorption bands of the adsorbed species gives a measure of the strength of the bond between the adsorbate and the adsorbing site [73]. Moreover, the specific frequencies of individual vibrational modes can probe the chemical nature of the surrounding catalytic environment.

The energy related to most of the molecular vibrations falls in the mid-infrared (MIR) region of the electromagnetic spectrum, and this is the reason for which the largest amount published papers reports spectra in this region, which ranges between 4000 and 400 cm^{-1}.

Another point is that the absorbance related to each molecular vibration is proportional to the abundance of the corresponding functional groups, hence the concentration of the species can be derived by the Beer-Lambert Law, Equation (2):

$$A = -log_{10}\, I/I_0 = \varepsilon \cdot l \cdot c \quad (2)$$

where A stands for the absorbance (dimensionless), and I and I_0 represent the intensity of the transmitted and incident light, respectively. The molar absorptivity ε parameter is expressed as $L \cdot mol^{-1} \cdot cm^{-1}$), the thickness of the sample l is reported in cm, and the molar concentration c is in $mol \cdot cm^{-1}$.

2.1. FTIR Spectroscopy of Adsorbed Probe Molecules

The surface sites in catalysts can be efficiently characterized by FTIR spectroscopy of probe molecules. FTIR spectroscopy is ideal for this approach, due to the specificity of the spectra for each adsorbate and to the high sensitivity to the kind of surface bonding to the local environment. The choice of the most appropriate probe molecule is therefore strategic: some probes are able to adsorb on specific sites, which can be detected and quantified, based on the intensity of the absorption. Other probes display different bonding on different sites, which can be identified by the corresponding changes in the IR spectra. Generally, the use of opportune molecular probes combined with FTIR absorption spectroscopy can provide information on:

(i) Acidic sites, in particular Brønsted sites, such as OH surface groups, and Lewis cationic sites. In this case, basic probe molecules as for example pyridine or other amines, NH_3, and acetonitrile are typically employed [74,75]. Moreover, the acid strength can also be determined by the shift observed in the O–H stretching region upon interaction by hydrogen bonding with weak basic probes, such as CO and NO [76,77].

(ii) Basic sites, normally surface oxygen atoms in oxides, CO_2 is usually employed, along with other probes less commonly used such as methanol [78], and also CO. CO_2 adsorption gives rise to the formation of mono- and bidentate carbonate species, hydrogen carbonates, and linearly-coordinated CO_2, providing detailed knowledge on the basic O^{2-} sites and M^{x+}–O^{2-} pairs (M^{x+} = metallic cation) [74].

Carbon Monoxide

A separate paragraph is dedicated to carbon monoxide because this molecular probe can be considered as the most versatile and clever probe [79]. Only vibrational modes with high cross-sections can be readily detected by FTIR spectroscopy, and this is among the reasons for which a large fraction of spectroscopic investigations concerns the adsorption of carbon monoxide (or other molecules containing C–O bonds). Indeed, besides providing information on the acidic and basic sites, the use of the CO probe offers knowledge on the nature of the metal catalytic sites, their oxidation state, and coordination mode [77,80,81]. In addition, CO can also be employed to determine the amount of sites with coordinative vacancies and available for catalysis. The CO molar absorptivity is commonly high, giving rise to strong IR signals for the C–O stretching mode in a frequency range almost without interference due to other species. The bands due to linear bonded CO can be observed in the 2000–2170 cm^{-1} range, whereas the position of those related to doubly bridged species is in the 1880–2000 cm^{-1} region, and multiply-bridged CO species give rise to bands below 1880 cm^{-1}. Moreover, the C–O stretching frequency is strongly dependant from the nature of the bond with the surface, i.e., from the electronic properties of the adsorbent site. Due to the small size, the CO molecule adsorption is ruled by steric hindrance effects. The frequency of the free molecule (2143 cm^{-1}) changes

when CO is adsorbed and such a shift is explained by the Bhyholder Model [82], in which the bond between the adsorbent site (a metal site) and CO is the result coming from two main contributions, which are shown in Figure 3. The first contribution is the σ donation that arises from the overlapping of the 5σ full orbital of the carbon atom (C, with weak anti-bonding nature) and of the empty d orbital of the metal site (M), which possesses dz^2 symmetry. The result of this overlapping is an electron density transfer from the CO molecule (lone pair on C atom) to M with an increase of the C–O bond strength. As a consequence, according to Equation (1), the ν_{CO} blue shifts with respect to the position of the free molecule.

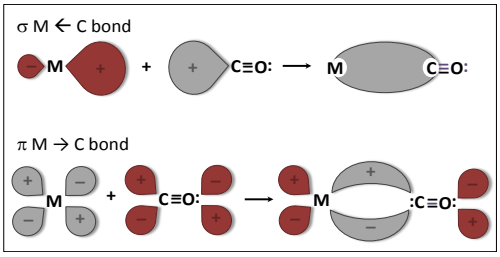

Figure 3. Metal atomic (M) orbitals and CO molecular orbitals involved in the adsorption.

The second contribution is the π back donation (dπ→pπ) with bonding character, resulting from the overlapping among two full d orbitals of M and the anti-bonding 2π* degenerate CO molecular orbitals. Such overlapping brings electron density in the anti-bonding CO orbital and the bond strength is decreased. Therefore, the position of the CO band red-shifts with respect to the free molecule. These two factors can predominate on each other based on the nature of the adsorbent: generally, σ donation is prevalent for metal ions with high oxidation state, on the contrary π back donation control the adsorption by neutral or partially negatively-charged metal atoms.

2.2. Experimental Setup

The experiments that are presented and discussed in this review have been carried out mainly in the mid IR frequency range, between approximately 700 and 4000 cm^{-1}, in which most of the molecular vibrations absorb light. Currently, Fourier transform infrared spectrometers (FTIR) are employed, and such instruments are fairly cheap and widespread in most analytical and research laboratories. In FTIR instruments a Michelson interferometer processes the collimated IR light before focusing it onto the sample and further collects and detects the resulting beam. According to Figure 4, the IR beam is split into two equal beams, the former is refracted in the direction of a fixed mirror, whereas the latter is transmitted to a movable mirror.

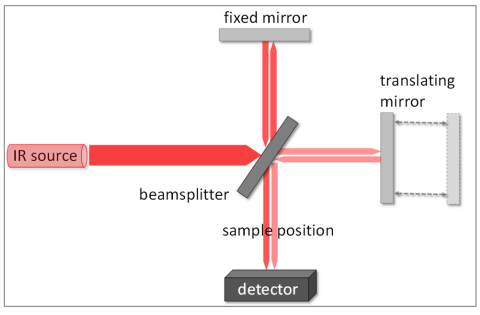

Figure 4. Schematic representation of a Michelson interferometer.

Then, these beams are recombined by the beam splitter and further directed toward the sample. The difference in optical path between the two beams is called retardation, and is varied over time by scanning the movable mirror. As a consequence, an interferogram is obtained by recording the signal

from the detector as a function of the retardation. The Fourier transformation of that signal provides the IR spectrum, which is reported as a function of the frequency.

Modern FTIR instruments are usually equipped by glow-bar IR lamps as the source and by mercury–cadmium–telluride (MCT) detectors for signal detection, due to the high sensitivity and to the capability to detect most of the mid IR frequency range. Due to the opportunity to collect simultaneously all wavelengths, higher signal-to-noise ratio can be achieved at a given scanning time. Moreover, the throughput is determined only by the diameter of the collimated IR beam. However, being a non-zero-background technique, FTIR instruments have limited sensitivity and glow-bar lamps should be replaced by synchrotron radiation or by tunable IR lasers [71].

Nevertheless, the widespread acceptance of IR absorption spectroscopy to efficiently characterize solid catalysts is mainly due to the availability of several experimental setups, which render the technique adaptable to a number of experiments that can be tailored on the nature of the sample to be investigated.

The most common experimental setups employed for catalyst characterization using IR absorption spectroscopy are (i) transmission FTIR mode, (ii) diffuse reflectance (DRIFTS) mode, (iii) attenuated total reflection (ATR) mode, in which the sample is placed in tight contact with a flat surface of the prism used to direct the IR beam, and (iv) reflection–absorption (RAIRS) mode, in which the IR beam is recoiled from a flat reflective surface before collection. This last setup is usually employed for model systems in surface-science studies. In this review, we will mainly focus on the transmission FTIR and diffuse reflectance (DRIFTS) common setups.

2.2.1. Transmission FTIR Mode

Most of the spectroscopic studies reported in the literature have been performed in transmission mode. Generally the setup consists in a self-sustaining pellet of the powered catalyst or of a mixture with IR transparent KBr, placed inside a cell allowing to work in controlled atmosphere, and collect in situ IR spectra [39,40]. A schematic picture of an example of transmission mode is shown in Figure 5. There is also the possibility to follow spectroscopically the catalytic reaction and to collect operando IR spectra.

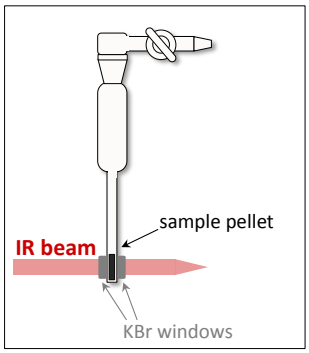

Figure 5. Transmission (TIR) mode, where the IR beam is directed through a self-sustained sample placed inside the catalytic reactor and collected after exiting for analysis.

Despite being quite popular, transmission mode setups undergo to the following constraints: the catalyst must be transparent to IR radiation in order to obtain spectra with reasonable intensity, the catalyst has to give the possibility to make thin self-sustaining pellets, and the intrinsic nature of the catalyst and the final sample form, such as pellets, depositions, and monoliths, can give serious problems for mass transport.

2.2.2. Diffuse-Reflectance (DRIFTS) Mode

To successfully overcome the problems arising from poorly transparent catalysts, or from samples not adequate to prepare a pellet, the diffuse-reflectance (DRIFTS) mode can be alternatively adopted. Here, the powdered sample is placed in a cell, where the interaction with the IR beam gives raise to scattered light, which is collected with appropriate optics (Figure 6). With this approach, the preparation of the sample is simpler than that with transmission FTIR. Due to this experimental setup, the intensity of DRIFT signal tends to be low and collecting good quality spectra becomes difficult. However, the intensity of the bands can be quite more enhanced when working in DRIFT mode with respect to the acquisition in transmission mode, due to the light multiple internal reflection close to the sample surface, resulting also in improved sensitivity towards the surface species rather than towards the gas phase species. On the contrary, the major drawbacks are related to the poor reproducibility due to the variations of scattering coefficients depending on the cell geometry, on the sample insertion procedure and on the occurrence of temperature gradient within the powdered sample with respect to the surface.

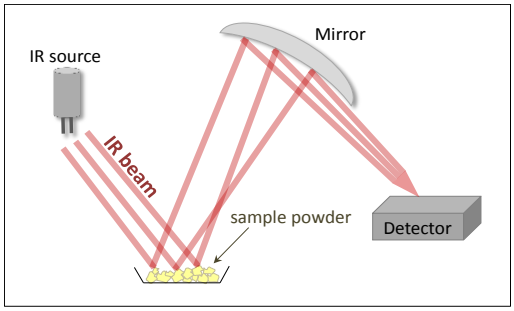

Figure 6. Diffuse reflectance (DRIFTS) mode, where an IR beam is focused on the powdered samples and the scattered light is collected by a parabolic mirror.

3. FTIR Spectroscopic Characterization: What Can Be Learned?

Usually, the use of FTIR spectroscopy is dedicated to the identification of the surface exposed sites of the catalyst to establish structure-activity relationships. Another application deals with the identification of the adsorbed species, and sometimes to their quantification and evolution during the reaction. In this review, we will try to center on some meaningful examples that shed light on open questions and improved the knowledge on the active sites involved in the H_2O_2 direct synthesis and on the parameters that have a beneficial effect on both conversion and selectivity.

3.1. Nature of the Active Sites on Pd Catalysts

Many studies focused on the identification of the nature and the role of Pd sites in promoting the direct synthesis of hydrogen peroxide from hydrogen and oxygen. In a very recent and interesting paper, Han et al. deduced that the active sites should not be properly represented by metallic or oxidized Pd species and elegantly pointed out that the active sites for the reaction originated from the interfaces among Pd and PdO domains on Pd/TiO_2 catalysts, as shown in Figure 7a [59]. The combined use of high resolution transmission electron microscopy (HRTEM), X-ray Diffraction (XRD), in situ diffuse reflectance Fourier Transform IR spectroscopy (DRIFT) of adsorbed CO, X-ray photoelectron spectroscopy (XPS), X-ray absorption near edge structure (XANES), and Extended X-ray Absorption Fine Structure (EXAFS) allowed to demonstrate that the structure of such Pd ensembles can be finely tuned by varying the Pd loading, while keeping constant the particle size. Indeed, the surface configuration of Pd atoms changed significantly for 1.0–5.0 wt% Pd loadings, whereas the size and the crystallinity of Pd particles remains unchanged. In situ DRIFTS spectra of adsorbed CO were collected on the Pd/TiO_2 catalysts with different Pd loadings to determine the surface structure and the results are shown Figure 7b.

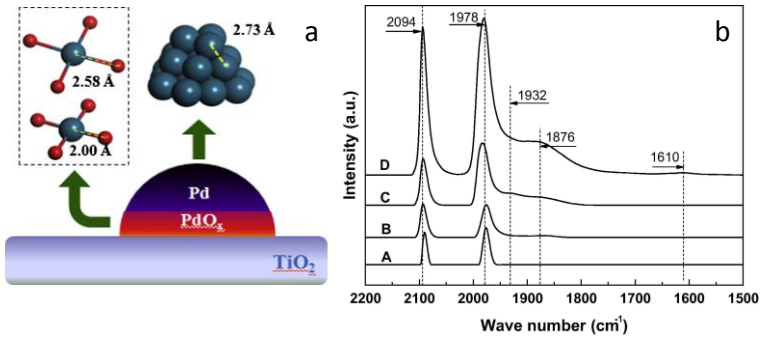

Figure 7. (**a**) Structural model of the Pd/TiO_2 catalyst. (**b**) In situ DRIFTS of CO adsorption over different catalysts at room temperature in an Ar flow (50 mL/min): A: 1.0% Pd, B: 2.0% Pd, C: 3.0% Pd, and D: 5.0% Pd. Reprinted from J. Catal., 321, L. Ouyang, P. Tian, G. Da, X. Xu, C. Ao, T. Chen, R. Si, J. Xu, Y. Han, The origin of active sites for direct synthesis of H_2O_2 on Pd/TiO_2 catalysts: Interfaces of Pd and PdO domains, 70–80, Copyright (2018), with permission from Elsevier.

The sharp peak at 2094 cm^{-1} is due to CO linearly adsorbed on low coordinated metallic Pd atoms located at the corners or at the edges of the nanoparticles. Moreover, the bands at 1978, 1932, and 1876 cm^{-1} are related to CO adsorbed on bridge and hollow sites of the Pd ensembles [83]. Such absorptions decreased in intensity by decreasing the Pd loading, however, the linear species/bridged and multibonded species ratio increases regularly. The intensity of the CO band at 1876 cm^{-1} was almost nil in the case of 1.0% Pd/TiO_2, which means that the increase of the Pd content induced the formation of continuous Pd ensembles exposing flat sites, thus lowering the amount of Pd corners or edges.

A rate in TOF of 630 h^{-1} along with 61% selectivity to H_2O_2 were obtained for the 1.0 wt% Pd catalyst at 283 K and 1 atm in a semibatch reactor. The reasons for the good catalytic performance were disentangled with the contribution of spectroscopic experiments focused on the Pd surface sites' reactivity that will be discussed in Section 3.3.

The origin of Pd particle size effects on H_2O_2 synthesis was rarely investigated [25,57]. It was reported that high metal dispersion of Pd nanoparticles supported on silica has a detrimental effect on the catalytic activity and selectivity towards H_2O_2 [31]. Moreover, shape-dependent catalytic activity of Pd nanocubes with {1 0 0} facets, and octahedrons with {1 1 1} facets was demonstrated [84]. The Pd octahedron shape gave rise to higher H_2O_2 selectivity and productivity than the catalyst with Pd cubes, therefore, suggesting that the Pd {1 1 1} facet is more active than the Pd {1 0 0} one. In another paper, {1 0 0} facet-enclosed Pd nanocubes of uniform shape, size, and crystallinity were prepared and supported on silica. It was found that the {1 0 0} Pd facet efficiently catalyzed H_2O_2 formation, however, it promoted side reactions, thus decreasing the selectivity [85].

In this frame, a series of size-controlled Pd/hydroxyapatite (HAp) catalysts ranging from single sites (Pd clusters) to nanoparticles (~30 nm) were synthesized and tested in H_2O_2 direct synthesis, showing up to 94% selectivity toward H_2O_2 formation when the Pd particle size is in the range 2.5–1.4 nm [57]. Extensive characterization by multi-technique approach was performed with the aim to obtain detailed information on the role played by crystal phase, morphology, surface electronic states, and coordination number of Pd particles (from atomic level to nanometers) and to establish a proper size range to obtain the best catalytic performances in the H_2O_2 direct synthesis. In particular, in situ CO DRIFT measurements were carried out to define the electronic structure of the surface Pd atoms and the spectra are shown in Figure 8a. Firstly, no vibrational band related to the HAp support was observed. The intensity of the peak at 2091 cm^{-1} related to CO linearly adsorbed on atop sites increased with decreasing the Pd particle size. Conversely, a gradual decrease in intensity of the absorption bands associated with CO adsorbed on bridged (1988–1964 cm^{-1}) and three-fold (1913–1873 cm^{-1}) sites was detected [83]. More in detail, the presence of the band at 2091 cm^{-1}, attributed to linear adsorbed CO, signalled the presence of highly dispersed Pd atoms and clusters

(0D and 2D particles) on the 0.5–2.0 wt% Pd catalyst. In addition, such a band did not change in intensity by increasing the Pd content. The authors inferred that the surface local environment of the HAp support strongly influenced the formation of these particles. Bands related to CO bridged species, growing in intensity with the Pd content, were detected on the 0.5 wt% Pd catalyst. These spectroscopic features, i.e., the bands observed in the 1913–1873 cm^{-1} range, due to CO adsorbed on Pd to hollow sites, pointed out the presence of Pd clusters, composed of high-density sites, or larger 3D Pd particles. In addition, the band due to linear carbonyls totally disappeared in the case of the 3.0 and 5.0 wt% Pd catalysts, suggesting that neither 0D nor 2D particles are present at the surface of these catalysts, due to Pd coalescence phenomena during the preparation.

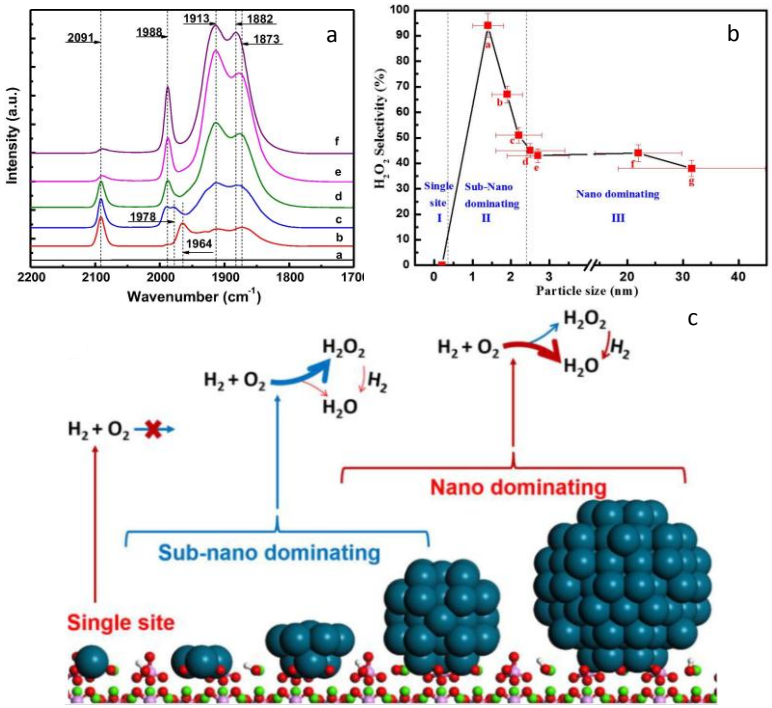

Figure 8. (**a**) In situ DRIFTS of CO adsorption over different catalysts at 283 K in an Ar flow (50 mL/min): a: HAp, b: 0.5 wt% Pd, c: 1.0 wt% Pd, d: 2.0 wt% Pd, e: 3.0 wt% Pd, and f: 5.0 wt% Pd. (**b**) Size dependence of H_2O_2 selectivity over Pd/HAp catalysts: a–e: catalysts calcined at 673 K with Pd loadings of 0.5, 1.0, 2.0, 3.0, and 5.0 wt%, respectively; f: 3.0 wt% Pd calcined at 773 K; g) 3.0 wt% Pd calcined at 873 K; (**c**) Structures of catalysts corresponding to three scales of particle sizes and proposed mechanism for H_2O_2 synthesis. Blue, red, white, purple, and green spheres are palladium, oxygen, hydrogen, phosphorus, and calcium atoms, respectively. Reprinted from J. Catal., 349, P. Tian, L. Ouyang, X. Xu, C. Ao, X. Xu, R. Si, X. Shen, M. Lin, J. Xu, Y.-F. Han, The origin of palladium particle size effects in the direct synthesis of H_2O_2: is smaller better? 30–40, Copyright (2017), with permission from Elsevier.

Based on the experimental findings in combination with DFT calculations, a structure–activity relationship by varying the Pd particle size was established (Figure 8b). Particularly, based on the Pd particle sizes and on the catalytic performance, three types of catalysts were identified: the first type is the single site catalyst (Pd(IE)), which is composed of atomically dispersed Pd species, and is almost inactive due to the lack of active sites (Figure 8c). The catalysts with 0.5–2.0 wt% Pd belong to type II, and are mainly made up by 2D and 3D Pd sub-nanoparticles with average size ranging from 1.4 to 2.5 nm (Figure 8c). According to the experimental results and the DFT calculations, these species are active in the H_2O_2 synthesis (Figure 8b), proving that the surface arrangement of Pd atoms plays a decisive role in the catalytic activity [86]. The 3.0–5.0 wt% Pd catalysts can be classified as the third type (Figure 8b,c), which is composed by large nanoparticles with size >2.5 nm, exposing mainly the

Pd(1 1 1) facets. The H_2O_2 formation is inhibited on these sites, due to the activity of metallic Pd towards O_2 dissociation, thus decreasing the selectivity.

The HAp support helped in keeping the size distribution of the Pd particles in a defined range, resulting in the formation of Pd particles with different geometric and electronic structures. In particular, the interaction between Pd and OH groups of HAp favoured the generation of sub-nanometer Pd species with a high $Pd^{\delta+}/Pd^0$ ratio. This was ascribed to be responsible of the remarkable improvement of H_2O_2 selectivity because the presence of $Pd^{\delta+}$ species lower the dissociative O_2 activation along with the H_2O_2 decomposition [59]. Hence, the Pd particles with sub-nanometer size are strongly interacting with the support and act as primary active sites.

3.2. Site Isolation and Electronic Effects

High dispersion of Pd sites as well as incremented Pd^0 content can boost the hydrogenation rate of hydrogen peroxide, however lowering H_2O_2 selectivity. Theoretical studies revealed the beneficial effect of Pd monomers, which favour H_2O_2 formation and, at the same time, avoid the O–O bond dissociation [87]. Ouyang et al. studied both H_2O_2 direct synthesis and side reactions over different Pd–Au/TiO_2 catalysts and discovered that the productivity of hydrogen peroxide increased by decreasing the Pd/Au ratio [86]. The in situ DRIFT spectra of CO adsorbed on Pd and Pd–Au catalysts, are reported in Figure 9a. Different metallic Pd sites were observed on the monometallic catalyst, and assigned to linear CO adsorbed on low coordination Pd atoms, presumably corners or edges of the nanoparticles (the band at 2096 cm^{-1}) [88], and to bridged and multibonded CO on Pd ensembles formed by two or three adjacent atoms (the bands at 1977, 1910, and 1851 cm^{-1}) [83].

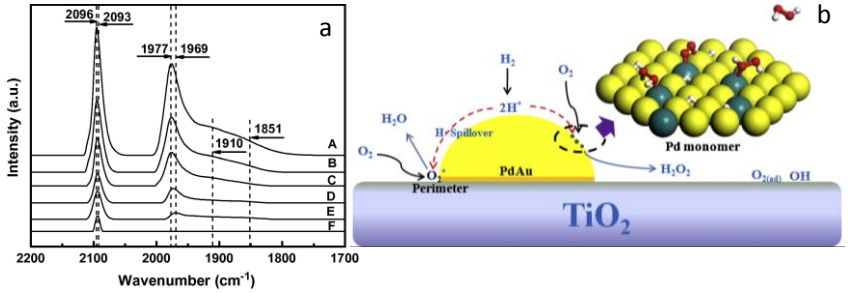

Figure 9. (**a**) In situ DRIFTS of CO adsorption over different catalysts at room temperature in streams of Ar with a flow rate of 50 ml/min. A: Pd, B: Pd2.5Au0.5, C: Pd2.0Au1.0, D: Pd1.5Au1.5, E: Pd1.0Au2.0, F: Pd0.5Au2.5. (**b**) Mechanism of H_2O_2 synthesis directly from H_2 and O_2 on a Pd monomer catalyst. Reprinted from J. Catal., 311, L. Ouyang, G. Da, P. Tian, T. Chen, G. Liang, J. Xu, Y.-F. Han, Insight into active sites of Pd–Au/TiO_2 catalysts in hydrogen peroxide synthesis directly from H_2 and O_2, 129–136, Copyright (2014), with permission from Elsevier.

Moreover, the intensity of these bands diminished dramatically by decreasing the Pd/Au ratio. Conversely, the ratio of the linear CO bands vs. bridged- and multi-bonded CO bands grew from 0.4 (monometallic Pd catalyst) to 1.0 (bimetallic Pd1.0Au2.0 catalyst). Based on these observations, the amount of surface Pd ensembles was lowered upon Au addition, whereas isolated Pd sites were increased (geometric effect occurring between Pd and Au), due to a dilution by gold. A small red-shift of the band related to the linear carbonyls, and a shift of the absorption of bridged carbonyls from 1977 to 1969 cm^{-1} were observed after Au addition. These shifts are possibly a consequence of the charge-transfer from gold to palladium, which enhanced the electron density of the involved d orbitals, resulting in a stronger back-donation to the 2π CO molecular orbitals. The authors suggested that molecularly adsorbed O_2 is activated without suppressing the O–O bond on Pd monomers embedded in low-coordinated Au sites to form H_2O_2 (Figure 9b). These Pd isolated sites are present at the surface of the homogeneous Pd–Au alloy observed by High Angle Annular Dark Field (HAADF)-TEM analyses. Conversely, the Pd ensembles favoured H_2O_2 hydrogenation. It was also proposed that the

sites at the interface between Au and TiO_2 are active in the H_2O formation directly from H_2 and O_2, because of the lowest selectivity and the absence of contiguous Pd ensembles.

The promotional effect of gold was previously reported for Pd–Au/SiO_2 catalysts by XPS measurements combined with in situ DRIFT spectroscopy of adsorbed CO. These studies proved the occurrence of surface and electronic modifications of Pd when alloyed with Au atoms, leading to enhanced reactivity and selectivity for the H_2O_2 direct synthesis [89]. Very recently, Flaherty et al. investigated Pd and Au_xPd_1 nanoparticles with similar size (7–11 nm) to understand the effect of alloying Pd with Au [90]. In particular, the aim was to find better explanations for the high H_2O_2 selectivity of these bimetallic catalysts by measuring the steady-state formation rates of both H_2O_2 and H_2O with respect to the pressure, the temperature, and the nature of the solvent. The authors indicated that H_2O_2 is produced by sequential surface proton-electron transfers. Interestingly, an increase of the Au:Pd ratio corresponds to different and simultaneous increases in the activation enthalpies related to the H_2O_2 and H_2O production. These changes are due to the occurrence of electronic changes induced by the addition of gold to palladium and are responsible for the improved selectivity towards H_2O_2 reported for AuPd bimetallic catalysts. The Pd and Au_xPd_1 were characterized also by FTIR spectroscopy, and the results are reported in Figure 10a.

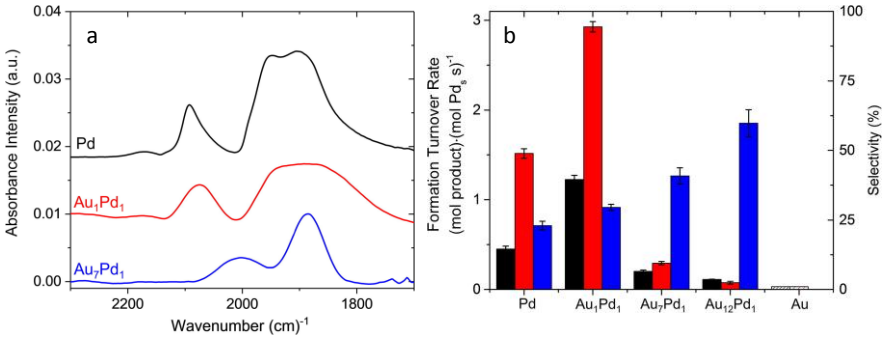

Figure 10. (**a**) Infrared spectra of CO adsorbed on Pd (black; 0.5 wt% Pd), Au_1Pd_1 (red; 0.5 wt% Pd), and Au_7Pd_1 (blue; 0.014 wt% Pd) obtained after saturating surfaces under flowing CO (~15 min in 5 kPa CO, 96 kPa He, 303 K) and purging gas-phase CO with He (101 kPa, 47.5 cm^3 min^{-1}, 303 K). Spectra are the average of 128 scans with a 4 cm^{-1} resolution. Peak heights were normalized by the atop bound CO feature at 2090–2000 cm^{-1}. (**b**) Steady-state H_2O_2 (black) and H_2O formation rates (red) and selectivity towards H_2O_2 (blue) on catalysts with different ratios of Au to Pd (55 kPa H_2, 60 kPa O_2, 305 K, 30 cm^3 min^{-1} 20% v/v methanol). Dashed bars indicate that rates were undetectable. Reprinted from J. Catal., 357, N. M. Wilson, P. Priyadarshini, S. Kunz, D. W. Flaherty, Direct synthesis of H_2O_2 on Pd and Au_xPd_1 clusters: Understanding the effects of alloying Pd with Au, 163–175, Copyright (2018), with permission from Elsevier.

The absorption bands in the 2090–2000 cm^{-1} range are assigned to atop CO species adsorbed on Pd, whereas those between 1960 and 1940 cm^{-1} are due to the formation of bridge bounded CO on Pd [83]. Upon gold addition to Pd, the peaks related to the atop carbonyl species are significantly red-shifted of about 90 cm^{-1} [91]. The ratio between the integrated areas of the bridge bounded/atop bands was taken as an indication of the relative amount of Pd ensembles with respect to Pd monomers [86], and decreased by adding Au to Pd, indicating the simultaneous presence of Pd and Au atoms within the same nanoparticle.

The formation turnover rates of H_2O_2 and H_2O are dependent on the Au content of the bimetallic Au_xPd_1 nanoparticles (Figure 7b). In particular, the formation rates of 0.11 mol H_2O_2 (mol Pd_s s)$^{-1}$ and 0.08 mol H_2O (mol Pd_s s)$^{-1}$ over the $Au_{12}Pd_1$ catalyst are lower than those obtained for the Pd catalyst (0.40 mol H_2O_2 (mol Pd_s s)$^{-1}$ and 1.4 mol H_2O (mol Pd_s s)$^{-1}$. Bare Au nanoparticles catalysed neither H_2O_2 nor H_2O formation, meaning that Pd is needed for the H_2O_2 direct synthesis and that Pd atoms are probably the active sites. Moreover, an enhancement of the selectivity towards H_2O_2 from 23% (bare Pd) up to 60% ($Au_{12}Pd_1$) was observed, since the decrease in H_2O formation at

increasing Au amount was larger than that of H_2O_2 at the experimental conditions reported in the paper (55 kPa H_2, 60 kPa O_2, 305 K). These observations were in agreement with the observed decrease of the bridge/atop CO ratio (Figure 7a), and with literature findings on AuPd nanoparticles supported on carbon [92], TiO_2 [27], and SiO_2 [89]. The increase in selectivity at increasing Au amounts was associated with greater activation enthalpies for H_2O_2 and H_2O production on isolated Pd atoms than on ensembles of Pd atoms [87].

With the aim of obtaining catalysts enriched with surface isolated Pd active sites for H_2O_2 synthesis, Zhang et al. [54] synthesized Pd-Zn bimetallic catalysts supported on alumina and with different Pd/Zn metal ratios. The 1Pd5Zn bimetallic catalyst reached 25,431 mol kg_{Pd}^{-1} h^{-1} of produced H_2O_2, which was superior than the productivity achieved in the presence of monometallic 1Pd catalyst (8533 mol kg_{Pd}^{-1} h^{-1}).

The authors bestowed the marked improvement of catalytic activity to geometric and electronic effects induced by Zn addition. XPS results indicated that at increasing Zn loadings the number of surface contiguous Pd sites decreased and, at the same time, an increase of the number of isolated Pd sites was observed. Indeed, Zn is able to disassemble the surface Pd agglomerates, thus enhancing the amount of Pd islands and single atoms [53]. The catalysts were reduced at 300 °C by using a 10% H_2/N_2 mixture for 60 min, and then cooled in a N_2 atmosphere before CO interaction at 30 °C for 15 min. The DRIFT spectra collected on monometallic Pd and on bimetallic PdZn catalysts are shown in Figure 11.

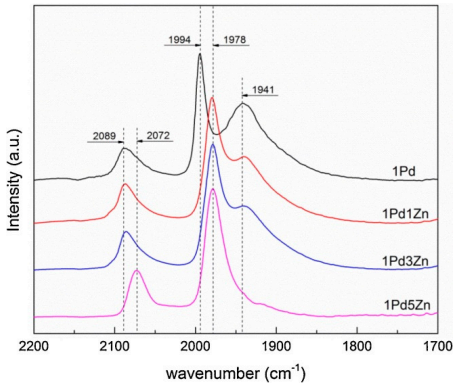

Figure 11. In situ DRIFTS of CO adsorption over different catalysts. Reprinted from Appl. Catal. A: General, 531, S. Wang, K. Gao, W. Li, J. Zhang, Effect of Zn addition on the direct synthesis of hydrogen peroxide over supported palladium catalysts, 89–95, Copyright (2017), with permission from Elsevier.

Bands at 2089 (linear CO adsorbed on isolated surface Pd sites [51]), 1994 (bridged CO species on Pd edges [93]), and 1941 cm^{-1} (bridged CO species on Pd atoms exposed at the surface of either (100) or (111) facets [39]) due to CO on different Pd sites were observed on the monometallic 1Pd catalyst [88]. Upon Zn addition, a red-shift of these peaks along with a gradual decrease in intensity of the peak at 1941 cm^{-1}, related to bridged carbonyls on Pd atoms on either (100) or (111) facets, was observed (red and blue curves), which almost completely disappeared in the case of the 1Pd5Zn catalyst (pink curve). These spectroscopic features put in evidence a strong Pd surface modification induced by the presence of Zn. In agreement with Ouyang et al. [86], the authors ascribed the observed red-shift to an increase of the electron density of the d-orbital due to the charge transfer from Zn to Pd species [86], resulting in an increase of the isolated Pd^0 sites amount. Indeed, the Pd-Zn electronic interaction positively promoted both H_2 conversion and H_2O_2 productivity.

Changes in surface composition and structure of bimetallic PdZn catalysts supported on silica were also already elegantly evaluated by Miller et al. using DRIFTS of CO adsorption combined with electron microscopy, X-ray absorption spectroscopy, CO chemisorption, and calorimetric analysis [53]. They observed the surface changes induced by varying the pre-reduction temperature from 225 up to 500 °C and reported the linear-to-bridge-bound ratio obtained by comparing the areas of the

peaks observed on two PdZn samples with different Pd:Zn molar ratios. The results are reported in Table 1. A significant increase in linear-bound CO was observed upon Zn addition, moreover the addition of a Zn excess zinc (2%Pd–10%Zn catalyst) resulted in a contained enhancement of the linear-to-bridge-bound CO ratio (2.5:1) with respect to the 3%Pd–1.8%Zn catalyst (2.1:1).

Table 1. Initial heat of CO adsorption values (±5 kJ/mol) in the presence of chemisorbed hydrogen and linear-to-bridge ratios from DRIFTS. Reprinted from J. Catal., 318, D. J. Childers, N. M. Schweitzer, S. Mehdi Kamali Shahari, R. M. Rioux, J. T. Miller, R. J. Meyer, Modifying structure-sensitive reactions by addition of Zn to Pd, 75–84, Copyright (2014), with permission from Elsevier.

Sample [1]	Reduction Temperature (°C)	CO (Initial) Heat of Adsorption with Chemisorbed H (kJ/mol CO) [2]	Linear-to-Bridge Ratio
$2Pd/SiO_2$ [3]	225	92	0.2:1
$2Pd–10Zn/SiO_2$	300	102	2.5:1
$3Pd–1.8Zn/SiO_2$	300	99	2.1:1
	550	93	1.8:1

[1] Catalysts were initially reduced under 5.11% H_2/Ar (both gases, 99.999% UHP) for 2 h at the specified reduction temperature, followed by subsequent cooling in H_2. [2] Initial heat of CO adsorption determined by microcalorimetry on a reduced Pd or PdZn surface containing chemisorbed hydrogen. [3] Monometallic Pd catalyst from previous work studied using the modified procedure.

The comparison of the DRIFT spectra of CO adsorbed on the 3%Pd–1.8%Zn catalyst pre-reduced at 300 and 550 °C (Figure 12a) put in evidence a shift from 2075 to 2070 cm^{-1} of the peak due to linear CO peak by increasing the reduction temperature at 500 °C, indicating a small increase of the population of linear carbonyls located at the Pd edge sites. Analogously, the absorption band related to bridge-bounded CO species showed a broadening and a shift from 1975 to 1965 cm^{-1} upon the increase of the reduction temperature. However, the linear-to-bridge ratio did not change significantly: from 2.1:1 at 275 °C to 1.8:1 at 550 °C.

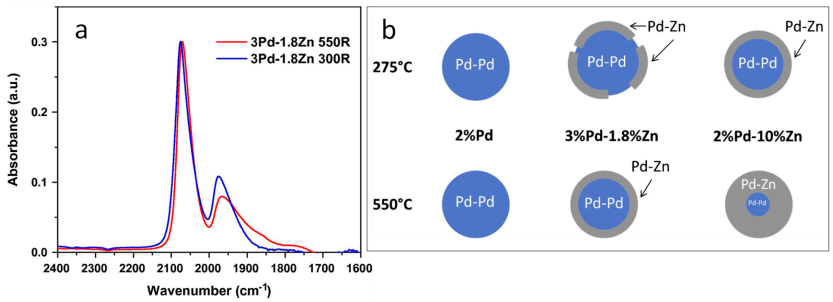

Figure 12. (**a**) Normalized DRIFT spectra of the 3%Pd–1.8%Zn catalyst pre-reduced at 300 °C (red) and at 550 °C (blue). (**b**) Cross-section of Pd and PdZn catalysts showing structure change as reduction temperature increased. Reprinted from J. Catal., 318, D. J. Childers, N. M. Schweitzer, S. Mehdi Kamali Shahari, R. M. Rioux, J. T. Miller, R. J. Meyer, Modifying structure-sensitive reactions by addition of Zn to Pd, 75–84, Copyright (2014), with permission from Elsevier.

Based on the characterization results, the authors proposed simplified models of the catalyst structure, which are shown in Figure 12b. In particular, the bimetallic nanoparticles of the 3%Pd–1.8%Zn catalyst have a Pd core with surface Zn atoms upon reduction at 275 °C, and the surface PdZn film possesses an intermetallic alloy structure, based on the high intensity of the band related to linear-bound CO bands. An increase in the surface PdZn intermetallic alloy, with few residual Pd ensembles, occurs at 550 °C, while the nanoparticle core is Pd-rich. This is due to the limited amount of Zn atoms interacting with Pd, resulting in the impossibility to form a fully intermetallic PdZn alloy nanoparticle at such temperature [94].

Conversely, in the case of the 3%Pd–1.8%Zn catalyst, a shell made up by PdZn alloy, totally covering the Pd-rich core was proposed already at 275 °C. For both catalysts, the PdZn metallic surface consists of an ordered alloy structure, and a random distribution of metallic Pd and Zn surface atoms is very unlikely. At 550 °C, there is almost complete formation of the PdZn alloy shell.

However, isolated Pd atoms were responsible for the enhancement of the catalytic activity and the authors ascribed this improvement to geometric effects rather than an electronic effect due to alloy formation.

An excellent Pd–Te/TiO_2 catalyst with almost 100% H_2O_2 selectivity under mild conditions (283 K, 0.1 MPa, using a semi-batch continuous flow reactor) was recently investigated [52]. Upon addition of tellurium, Pd nanoparticles with smaller size were obtained, and such Te-modified Pd surfaces hindered the O_2 dissociative activation, favouring at the same time the non-dissociative O_2 hydrogenation. In order to find structure–activity relationships, DRIFT spectroscopy of adsorbed CO was employed in combination with STEM-EDS, EXAFS, O_2-TPD, XPS, and DFT calculations to shed light on the electronic structure of the surface Pd atoms.

As shown in Figure 13a, the band ascribed to CO linearly adsorbed on Pd sites red-shifted from 2079 to 2051 cm^{-1} upon addition of Te. Moreover, according to DFT calculations, the binding energy of CO adsorbed on low-coordinated Pd sites exposed at the surface of smaller particles was noticeably higher than that related to CO adsorbed on the Pd terrace sites of extended surfaces. Particularly, the amount of smaller Pd nanoparticles increased at increasing Te loading, resulting in an increase of the low-coordinated Pd corners and edges, as indicated by the enhancement of the intensity of the band related to linearly carbonyls and by the gradual decrease of the absorption centred at 1982–1902 cm^{-1} ascribed to CO on bridge and hollow sites [83]. Indeed, only the band related to CO linearly bounded was present in the case of the $Pd_{17}Te_4$ and Pd_3Te_2 catalysts, confirming the presence of highly dispersed clusters or isolated Pd atoms.

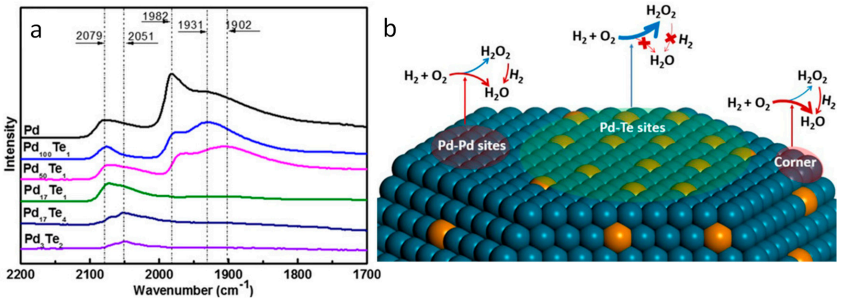

Figure 13. (**a**) In situ DRIFTS measurement of CO adsorption over the Pd–Te/TiO_2 catalysts at 283 K in an Ar flow. (**b**) Proposed mechanism for the direct synthesis of H_2O_2 over Pd–Te/TiO_2 catalysts. Blue and brown spheres are Pd and Te atoms, respectively. Reprinted from P. Tian, X. Xu, C. Ao, D. Ding, W. Li, R. Si, W. Tu, J. Xu, Y.-F. Han, ChemSusChem, 10, 3342–3346, Copyright (2017), John Wiley and Sons.

A mechanism explaining the role of Te in improving the catalytic activity was proposed based on STEM-EDS, EXAFS, and CO-DRIFTS results. In particular, the reason for the noticeable catalytic performance was ascribed to the presence of selectively active sites bimetallic Pd–Te, in which the Te inertness toward O_2 adsorption significantly inhibited the dissociative O_2 activation as revealed by XPS and O_2-TPD analyses. As a matter of fact, the $Pd_{150}Te_1$ catalyst containing poor Te amount showed higher selectivity than the monometallic Pd catalyst. Side reactions were noticeably inhibited and a selectivity of almost 100% was achieved by increasing the Te/Pd atomic ratio to 1:100, because of the increased number of surface Pd–Te sites. Indeed, a much contained increase of the Te/Pd ratio to 1:50 and 1:17 resulted to lower selectivity (78.8% and 67.3%, respectively).

At the same time, as indicated by XRD, TEM, and CO-DRIFTS findings, the Pd particle size was diminished at increasing Te/Pd ratios, and low-coordinated active edges and corners were formed. Such low-coordinated sites are much more active to bind and dissociate molecular O_2, with respect

to terrace sites [95]. As a result, the selectivity to H_2O_2 of the $Pd_{50}Te_1$ and $Pd_{17}Te_1$ catalysts is lower than that observed in the case of $Pd_{100}Te_1$. Thus, a high amount of surface Te sites would inhibit both H_2 and O_2 reactant molecules adsorption, resulting in inert $Pd_{17}Te_4$ and Pd_3Te_2 materials. Indeed, the surface Pd atoms of these catalysts are isolated by Te atoms, as revealed by EXAFS and CO-DRIFTS. The results indicate that only by finely tuning the Pd/Te ratio it is possible to control the amount of terrace Pd-Te sites, as well as the particle size to obtain highly-performing catalysts.

Very recently Flaherty et al. reported that the steady-state selectivity to H_2O_2 of AgPt octahedra supported on silica (50%) is 10-fold greater than observed with Pt/SiO_2 nanoparticles with similar size (6%) [45]. In addition, the abundance and location of Pt atoms on the AgPt octahedra surface play a role on the initial formation rates selectivity to H_2O_2. The population of these sites can be modulated either by CO exposure at 373 K to obtain a Pt-rich surface (with 16% initial H_2O_2 selectivity) or by inert gases exposure at the same temperature to achieve a Pt-poor surface (with 36% initial H_2O_2 selectivity).

FTIR experiments of adsorbed ^{12}CO were then performed on the monometallic Pt catalyst and on the AgPt catalyst pretreated in ^{12}CO or He (Figure 14a). Firstly, it has to be recalled that ^{12}CO does not adsorb on the Ag sites under the adopted experimental conditions. The bands of adsorbed ^{12}CO on $AgPt_{CO}$ (black curve) and $AgPt_{He}$ (red curve) octahedra differ significantly in both position and intensity, due to modifications of surface structure of the AgPt octahedral, because the FTIR spectra were obtained by submitting the same sample pellet to in situ CO and He pre-treatments. Conversely, the band at 2098 cm^{-1} was assigned linear carbonyl species adsorbed on single Pt atoms exposed at the surface of the nanoparticles [96] and on Pt(111) [81]. The positions of the bands related to linearly adsorbed ^{12}CO are significantly red-shifted at 2051 cm^{-1} for $AgPt_{CO}$ and at 2033 cm^{-1} in the case of $AgPt_{He}$, revealing different extents of electron exchange between the ^{12}CO probe. Such a feature can be ascribed to lower dipole–dipole coupling between the ^{12}CO molecules due to the lower coverage of linear carbonyls, which results in a red-shift of the ^{12}CO band [81]. In addition, the intensity of the peaks related to the AgPt octahedra pre-treated with CO was about six times the intensity observed for $AgPt_{He}$, which pointed out that the ^{12}CO pre-treatment was able to extract a much bigger amount of exposed Pt sites at the surface of the AgPt octahedra with respect to the treatment in He. Moreover, the difference in position of about 20 cm^{-1} for $AgPt_{CO}$ and $AgPt_{He}$ was in agreement with the literature on CO adsorbed on well-coordinated Pt terraces and on under-coordinated Pt edges [96].

In order to verify the occurrence of different electronic effects on the catalysts, the singleton frequency can be evaluated by using ^{13}CO–^{12}CO isotopic mixture to dilute the adsorbed ^{12}CO molecules and by evaluating of exchange rates between adsorbed ^{13}CO and ^{12}CO. The changes in the singleton frequency of adsorbed ^{13}CO clearly pointed out the electronic changes in Pt atoms as shown in section b of Figure 14. In particular, a red-shift of the band related to adsorbed ^{13}CO was observed by decreasing the ^{13}CO coverage (θ^{13}_{CO}), signifying the occurrence of dipole–dipole coupling. The ^{13}CO singleton frequency was calculated by extrapolation of the spectra (shown in section a) to a zero coverage, and obtaining 2016 $\pm$ 6 cm^{-1} for the monometallic Pt catalyst, 1974 $\pm$ 8 cm^{-1} for $AgPt_{CO}$, and 1979 $\pm$ 12 cm^{-1} for $AgPt_{He}$. The last two values were much lower than on the Pt catalyst, which indicates a greater extent of electron back-donation from the Pt atoms to the CO $2\pi^*$ orbitals on the AgPt octahedra. The above findings were unexpected, since the AgPt octahedra gave higher selectivity to H_2O_2 than Pt nanoparticles.

The isosteric ^{13}CO desorption under ^{12}CO flow on $AgPt_{He}$, $AgPt_{CO}$ and on Pt nanoparticles are reported in Figure 14, section c. It can be observed that the ^{13}CO desorption and exchange with ^{12}CO take 400 s on Pt, whereas only about 50% and 15% ^{13}CO exchange occurs in 800 s on $AgPt_{He}$ and $AgPt_{CO}$, respectively. The ^{13}CO desorption rates were described by Equation (3), a first-order desorption process for surfaces containing n adsorbing sites:

$$-\frac{d\theta_{13CO}}{dt} = \sum_{i}^{n} k_i \cdot \theta_{13CO,i} \quad (3)$$

where k_i is the rate constant for CO desorption from site i expressed in s^{-1}. The sum of all coverages $\theta^{13}_{CO,I} = 1$ at the exchange onset. The desorption rates for >95% of ^{13}CO molecules from the surfaces of the Pt nanoparticles were accurately delineated by a model that describes a uniform surface for which $n = 1$. This was not true in the case of $AgPt_{He}$ and $AgPt_{CO}$ octahedral, because two distinct sites have to be considered to explain the desorption kinetics and the significant ^{13}CO amount that remain adsorbed during the experiment. H_2O_2 and H_2O form on distinct active sites and the ratio between those on which H_2O_2 is formed and those on which H_2O formation occurs increased upon Ag addition.

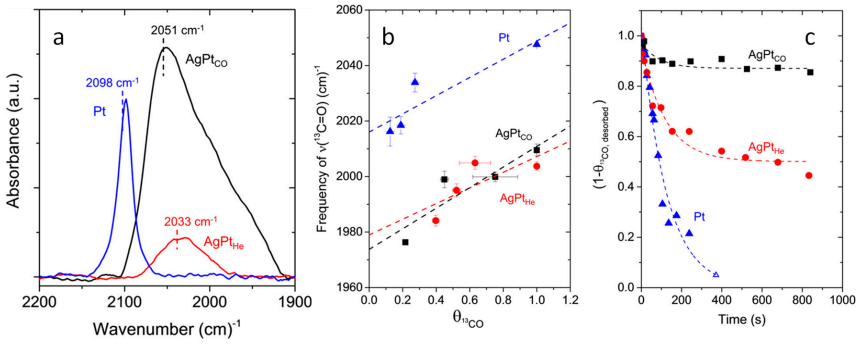

Figure 14. (**a**) infrared spectra of adsorbed ^{12}CO following the purge of gas-phase ^{12}CO with He (101 kPa, 30 cm^3 min^{-1}, 303 K) on Pt (blue), $AgPt_{CO}$ (black), and $AgPt_{He}$ (red). Spectra are the average of 128 scans with a 4 cm^{-1} resolution. Dotted lines are intended to show the peak position for each spectrum. (**b**,**c**) Peak position of $\nu_{(C=O)}$ for ^{13}CO as a function of the coverage of adsorbed ^{13}CO (θ^{13}_{CO}) (total of 1 kPa CO, 100 kPa He, 100 cm^3 min^{-1}, 298 K) and change in the coverage of θ^{13}_{CO} as a function of time during exchange with ^{12}CO on Pt (blue triangles) and CO-treated (black squares) and He-treated (red circles) AgPt octahedral particles (0.2 kPa ^{12}CO, 100 cm^3 min^{-1}, 298 K; surfaces pre-saturated with ^{13}CO). Solid lines in (**b**) represent a linear fit to the data, and dashed lines in panel c represent the fit of θ^{13}_{CO} as a function of time. Adapted with permission from ACS Catalysis, N. M. Wilson, Y.-T. Pan, Y.-T. Shao, J.-M. Zuo, H. Yang, D. W. Flaherty, Direct Synthesis of H_2O_2 on AgPt Octahedra: The Importance of Ag–Pt Coordination for High H_2O_2 Selectivity, 8, 2880–2889. Copyright (2018) American Chemical Society.

3.3. Reactivity of the Exposed Metal Sites

Only few studies proposed in situ approaches to investigate by FTIR spectroscopy of adsorbed probes the reactivity of the metallic active sites upon interactions with the reagents, i.e., molecular hydrogen and oxygen or mixtures of the two. It is worth noting that the reagents involved in the H_2O_2 direct synthesis are IR inactive, because there is no change in the dipole moment of the molecules upon interaction with the IR radiation.

One very recent example on this approach is reported in the study by Han et al. [58], which has been already discussed in Section 3.1 as for the nature of the Pd sites on Pd/TiO_2 catalysts. In addition to the common investigation carried out by adsorbing the CO probe, the authors characterized the catalysts submitted to subsequent adsorption of molecular oxygen and hydrogen, before the inlet of the CO probe. Indeed, the surface of the freshly reduced catalyst dramatically changed upon O_2 preadsorption: the narrow peak at 2094 cm^{-1} due to the linear carbonyls (see Figure 7b) was transformed into two weak peaks at 2090 and 2064 cm^{-1} (Figure 15). Moreover, bridged and multibonded CO species on Pd ensembles red-shifted to 1986, 1914, and 1874 cm^{-1}, and also the relative intensities were modified, due to the geometric and electronic modification of Pd atoms induced by oxygen adsorption. Such changes were accompanied by an increase in intensity of the band at 1646 cm^{-1} due to the formation of carbonate species.

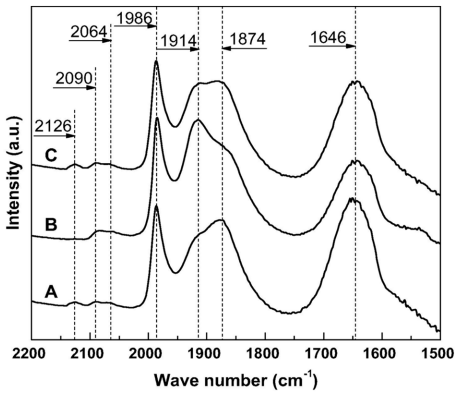

Figure 15. In situ DRIFTS of CO adsorption over the reduced 1.0% Pd catalyst: A: pretreatment with O_2, adsorption of CO and purged with Ar; B: H_2 treatment of A, readsorption of CO and purged with Ar; C: O_2 retreatment of B, readsorption of CO and purged with Ar. All the experiments were carried out at 283 K. Reprinted from J. Catal., 321, L. Ouyang, P. Tian, G. Da, X. Xu, C. Ao, T. Chen, R. Si, J. Xu, Y. Han, The origin of active sites for direct synthesis of H_2O_2 on Pd/TiO_2 catalysts: Interfaces of Pd and PdO domains, 70–80, Copyright (2018), with permission from Elsevier.

At the same time a new band at 2126 cm^{-1}, probably due to CO on positively-charged Pd formed after oxygen pre-adsorption and the broad and complex absorption at 1800–2000 cm^{-1} remained unchanged. Upon H_2 contact for 5 min the band at 1646 cm^{-1} decreased in intensity and the peak at 2126 cm^{-1} was totally depleted, pointing out the reduction of the positively-charged Pd sites. The intensity of these absorptions was completely recovered after further O_2 inlet for 5 min and re-adsorption of CO, which is an indication of partial oxidation of the surface Pd atoms. This behaviour suggested that the electronic structure of the surface Pd atoms undergoes to dynamical changes during the reaction as a consequence of the interaction and adsorption of molecular oxygen and hydrogen reactants. Moreover, the comparison with the CO bands observed in the presence or in the absence of oxygen (Figure 7a), allowed understanding that oxygen is preferentially adsorbed on the Pd corners or edges sites, according to the marked decrease in intensity of the bands related to linearly adsorbed CO. At the same time, oxygen is also adsorbed on the flat sites of the Pd particles, as revealed by the change occurred on the bands assigned to CO adsorbed on Pd continuous ensembles. Therefore, the Pd corner or edge sites, which are highly reactive towards oxygen dissociation are modified by adsorbed oxygen species or are partially oxidized to PdO, which weakens the O_2–Pd interaction. Such modification positively influenced the molecular O_2 activation and the further H_2O_2 synthesis, which is assumed to occur at the interface of the Pd and PdO domains.

The characterization results showed that a fraction of the surface Pd atoms can be easily oxidized at 283 K (47.6% for the 1.0 wt% Pd catalyst and 35.2% for the 5.0 wt% Pd one), and form Pd–PdO ensembles. The electronic structure of the surface Pd atoms has proved to change dynamically in different atmospheres. The experimental results presented in the paper clearly demonstrated that the structure of supported Pd active sites can be tuned by choosing opportunely the metal loading while the size of the metal particles is unchanged. Therefore, the variation of the metal loading does not correspond to a simple increase in the number of active sites, but it is an effective approach to tune the structure of the active sites. These insights into the Pd–PdO–TiO_2 interface greatly contributed to understand the active phase geometric and electronic structure and the mechanism for direct H_2O_2 synthesis.

Strukul et al. previously observed that surface oxidized monometallic Pd and bimetallic Pd-Au catalysts pretreated with H_2 and O_2 displayed higher activity and selectivity than the untreated samples [97]. Moreover, even though gold itself is not active, both productivity and selectivity were improved by Au addition. The catalysts with different supports have been tested the H_2O_2 direct synthesis under very mild and non-explosive conditions (1 bar, 20 °C). The catalysts supported on

sulphated zirconia (ZS) gave the best performance (1270 mmol H_2O_2/gPd h after three hours of reaction, with 61% selectivity) in the presence of H_2/O_2 mixtures with a large excess of oxygen (4/96).

HRTEM measurements indicated that gold and palladium were in close contact and FTIR spectroscopy was employed to (i) monitor the nature and the electronic properties of the Pd sites upon Au addition, and (ii) the reactivity of these sites after pretreatment in O_2 and/or H_2 atmosphere. CO was adsorbed at room temperature on the ZS-Pd and ZS-PdAu catalysts and the results are compared in Figure 16a,b, respectively. The FTIR spectra were collected on the untreated catalysts (bold curves), on those submitted to H_2 pre-treatment at room temperature (fine curves), and on the catalysts pre-treated with H_2 and O_2 (dashed curves).

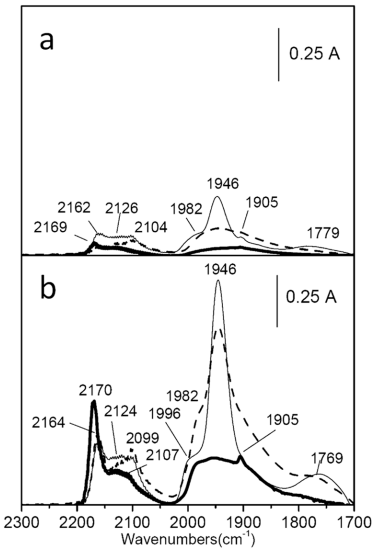

Figure 16. FTIR spectra of ZS–Pd (**a**) and ZS–PdAu (**b**) after CO adsorption at r.t on the as received samples (bold curves), on the samples pretreated at room temperature with hydrogen (fine curves) and pretreated with hydrogen and oxygen (dashed curves). The spectra have been normalized to the same Pd content. Reprinted from J. Catal., 257, F. Menegazzo, P. Burti, M. Signoretto, M. Manzoli, S. Vankova, F. Boccuzzi, F. Pinna, G. Strukul, Effect of the addition of Au in zirconia and ceria supported Pd catalysts for the direct synthesis of hydrogen peroxide, 369–381, Copyright (2008), with permission from Elsevier.

Different bands in the range of linear (2200–2000 cm^{-1}) and bridged (2000–1700 cm^{-1}) CO carbonyl species were observed upon CO adsorption have been detected [98]. The ZS-Pd and ZS-PdAu catalysts possess very similar spectroscopic features: all the produced bands were related to Pd carbonyl species, no bands due to CO on Au sites were observed for the bimetallic catalysts, and the intensity of the CO bands produced on the ZS-PdAu sample was much higher than that related to the bands observed for the monometallic catalyst, independently from their pretreatments.

FTIR spectroscopy pointed out that in the bimetallic catalysts the Pd dispersion was higher, in agreement with HRTEM results. In addition to the increased number of active sites, a high metal dispersion can modify the interaction with oxygen, strongly affecting the selectivity. It was reported that oxygen cannot dissociate on the very small metallic clusters, due to the repulsive effects between the two negatively-charged O atoms [99]. Upon H_2 pre-treatment, the band at 1946 cm^{-1} observed for both mono- and bimetallic catalysts (fine curves), and assigned to CO adsorbed on bridge-bonded CO on Pd terrace sites of (111) facets [100], increased in intensity. Conversely, this band was almost completely depleted after interaction with the H_2–O_2 mixture on ZS–Pd (Figure 16a, dashed curve), and slightly decreased in intensity on ZS–PdAu (Figure 16b, dashed curve). This behaviour indicates that on ZS–PdAu a large fraction of the terrace sites was preserved after oxidation, resulting in a less defective and less energetic surface. Moreover, in the case of the ZS–PdAu catalyst, the intensity of

the absorption at 1770 cm^{-1} was maximum, due to a larger back-donation from the metal to the CO probes, as a result of an electronic effect of gold on palladium.

The presence of gold in close proximity of palladium was therefore proposed based on the changes in the electron density induced on Pd sites evidenced by FTIR and in the morphology observed by HRTEM.

The authors investigated the effect of the H_2–O_2 pre-treatment at room temperature on the surface oxidation state of the bimetallic catalysts by FTIR of CO absorption (Figure 17). Firstly, the intensity of the CO bands observed for the AuPd catalyst supported on ceria (CeS–PdAu, orange curve) was quite weak, analogously to what observed on the same sample simply outgassed at room temperature (data not shown). However, in this case the on top CO linear species/bridged CO species intensity ratio obtained without pre-treatment and after H_2–O_2 interaction was quite similar, which indicates a contained decrease of the exposed sites and no changes in their nature and relative abundance.

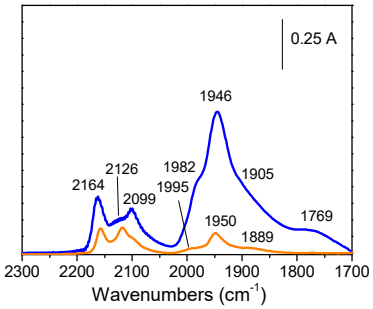

Figure 17. FTIR spectra of CO adsorbed at r.t. on the ZS–PdAu (blue curve) and CeS–PdAu (orange curve) samples previously contacted with a H_2–O_2 mixture at room temperature. The spectra have been normalized to the same Pd content. Reprinted from J. Catal., 257, F. Menegazzo, P. Burti, M. Signoretto, M. Manzoli, S. Vankova, F. Boccuzzi, F. Pinna, G. Strukul, Effect of the addition of Au in zirconia and ceria supported Pd catalysts for the direct synthesis of hydrogen peroxide, 369–381, Copyright (2008), with permission from Elsevier.

Conversely, the overall intensity of the bands observed for the ZS–PdAu catalyst (blue curve) was much stronger. In addition, the linear/bridged intensity ratio was much higher for ZS–PdAu with respect to CeS-PdAu. This spectroscopic feature is due to the different nature of the two supports. Ceria can be quite easily reduced at the interface with the metallic particles under mild conditions, which results in the production of oxygen vacancies, and migration of oxygen on the small metallic particles [84]. Moreover, on this catalyst a large fraction of the Pd sites was present as PdO, on which CO does not adsorb, upon H_2–O_2 treatment [101]. PdO species formation takes place preferably at the particle/support interface, whereas the Pd atoms located on top of the particle, far from the interface between the metal and the oxide keep on being metallic when the particle size is >3 nm [102]. In this frame, the nature of the support strongly affected both the formation and stabilization of oxidized particles.

Such process was promoted on the ceria support because of its oxygen storage-release properties along with the smaller size of the metallic particles detected on both the Pd and PdAu catalysts supported on CeS catalysts, according to the HRTEM observations.

Based on the characterization results, a reaction mechanism for the Pd and Pd-Au bimetallic catalysts was proposed depending on the nature of the active metallic sites, i.e., less energetic and more energetic sites [103]. As illustrated in Figure 18, in the former case, H_2O_2 direct synthesis occurs by: (i) oxygen activation without dissociation on non-defective (less energetic) Pd sites, followed by (ii) protonation external H^+, and (iii) reaction with molecular H_2 to form H_2O_2 with H^+ restoration. On the contrary, O_2 is chemisorbed by dissociative way on defect, edge, and corner sites (more energetic sites), which are able to re-adsorb H_2O_2. Thus, due to the presence of chemisorbed H_2, water can be formed by reaction with oxygen atoms or with the OH fragments coming from H_2O_2.

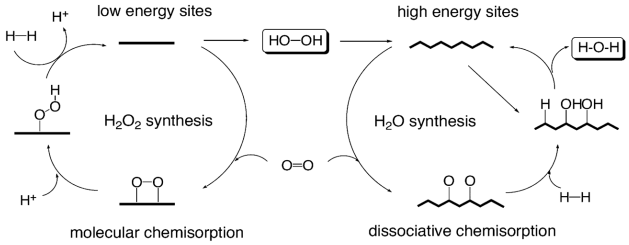

Figure 18. Possible pathway for the synthesis of H_2O_2 and H_2O on mono- and bimetallic Pd–Au catalysts. Reprinted from J. Catal., 257, F. Menegazzo, P. Burti, M. Signoretto, M. Manzoli, S. Vankova, F. Boccuzzi, F. Pinna, G. Strukul, Effect of the addition of Au in zirconia and ceria supported Pd catalysts for the direct synthesis of hydrogen peroxide, 369–381, Copyright (2008), with permission from Elsevier.

Therefore, upon gold addition of gold, the amount of terrace sites (less energetic sites) increased along with the selectivity to H_2O_2. However, as pointed out by FTIR measurements, the amount of more energetic active sites did not rise, as expected. The active phase of Pd–Au bimetallic catalysts was confirmed to be made up by a core-shell morphology with an Au-rich core/Pd-rich shell morphology and a Pd-rich surface according to the studies by Hutchings et al. [26,27,41,104–106]. The occurrence of an electron donation from the Au core to the Pd shell, which results in less reactive sites toward O_2 dissociation, was demonstrated by the presence of the band at 1770 cm^{-1}. Gold was proven to have a complex role, since it improves the Pd catalytic activity by decreasing the size, morphology and electron density of the Pd particles.

In a following paper by the same authors, the effect of the morphological and composition properties of differently prepared Pd–Au catalysts supported ZrO_2 on the direct synthesis of hydrogen peroxide was investigated [39]. It was shown that the consecutive deposition of gold by deposition-precipitation and then of palladium by incipient-wetness impregnation allowed to prepare catalysts (1Au2Pd) with a H_2O_2 productivity at pressure corresponding to 18,000 $mmol_{H_2O_2}/g_{Pd}h$ with 59% selectivity, unusually higher than that observed at atmospheric pressure. Moreover, large roundish bimetallic particles with an Au/Pd ratio ranging from 0.3 up to 1.5, as determined by EDS analysis, were mainly observed on the 1Au2Pd catalyst. To obtain more insight on the surface sites, CO adsorption was performed at 180 K in order to observe also the $Pd^{\delta+}$ carbonyl species, which do not chemisorb the probe at room temperature. Indeed, CO bands at 2160 cm^{-1} and 2135 cm^{-1} signalled the presence of Pd^{2+} ions stabilized by chloride ions coming from the metal precursor [107] and of $Pd^{\delta+}$ at the surface of oxidized Pd^0 particles [108] on the catalysts simply outgassed for 1 h at room temperature (data not shown). The FTIR spectra of CO adsorbed on Pd (Figure 19a), 1Au2Pd (Figure 19b), 1Pd2Au (Figure 19c), and PdAu (Figure 19d) submitted to H_2 pre-treatment at room temperature (fine curves) and to subsequent interaction with H_2, then O_2 atmosphere at the same temperature (bold curves) are compared in Figure 19.

Generally, the spectra display similar band positions, which are in the range of on top, two-fold bridged or three-fold bridged Pd^0 carbonyls. A band at 2169 cm^{-1}, related to CO adsorbed on Zr^{4+} sites of the support, was detected for the 1Pd2Au catalyst (Figure 19c). Moreover, the spectra differed as for the overall intensity, and those related to the 1Au2Pd catalyst had the lowest intensity, which suggests the presence of large particles, in agreement with the results of the HRTEM analysis. The pre-treatment in H_2 and O_2 atmosphere (bold curves) induced a marked decrease in intensity of the spectra for all samples, pointing out that a surface oxide layer, exposing sites unable to adsorb the probe, was formed [108,109]. In particular, a 95% intensity band decrease of all carbonyls was observed on the 1Au2Pd sample (Figure 19b), and ascribed to electronic and chemical effects induced by Au on the Pd sites. A curve fitting procedure of the experimental spectra collected after H_2 and O_2 pre-treatment was carried out and the obtained deconvolutions are shown in Figure 20. Linear CO species adsorbed on Pd^0 sites of (1 1 1) facets (band at 2108 cm^{-1}), bridged CO on Pd^0 edge sites (1999 cm^{-1}), bridged CO species on Pd^0 sites of (1 0 0) or (1 1 1) facets (band observed at 1941 cm^{-1}),

and CO species on different threefold hollow Pd sites (bands at 1880 and 1809 cm^{-1}) were observed for the Pd monometallic catalyst [110].

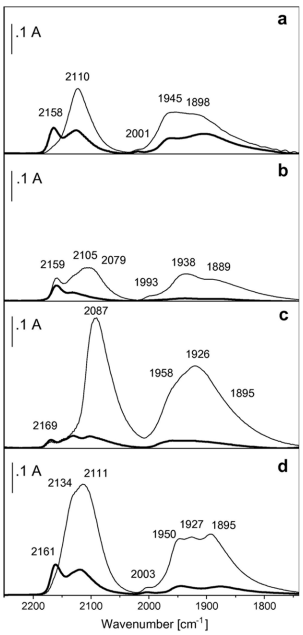

Figure 19. FTIR spectra of CO adsorbed at 180 K on Pd (**a**), 1Au2Pd (**b**), 1Pd2Au (**c**), and PdAu (**d**) after pre-treatment in H_2 at room temperature (fine curves) and after pre-treatment in H_2 and O_2 at r.t. (bold curves). Reprinted from J. Catal., 268, F. Menegazzo, M. Signoretto, M. Manzoli, F. Boccuzzi, G. Cruciani, F. Pinna, G. Strukul, Influence of the preparation method on the morphological and composition properties of Pd–Au/ZrO_2 catalysts and their effect on the direct synthesis of hydrogen peroxide from hydrogen and oxygen, 122–130, Copyright (2009), with permission from Elsevier.

Upon the same hydrogen–oxygen pre-treatment, carbonyls on Pd^{2+} and $Pd^{\delta+}$ (2160 and 2134 cm^{-1}) and CO adsorbed on different Pd sites (weak components at 2104, 1985, 1941, and 1879 cm^{-1}) were detected for the most performing 1Au2Pd catalyst (Figure 20b). The low intensity of such absorption pointed out that the O_2 reactant molecule can easily oxidize the Pd sites present in this catalyst due to the electronic effect induced by gold on the Pd atoms, due to the higher electronegativity of gold (2.54) with respect to that of palladium (2.2) [111]. Moreover, the red-shift observed for the bands at 2104 (small shift) and 1985 cm^{-1} (large shift) with respect to the same carbonyls of the Pd catalyst was ascribed to lateral interaction effects, suggesting the presence of more isolated sites on the 1Au2Pd catalyst. This was a consequence of the alloying of the two metals and not of the smaller size of the particles. Thus, the band at 1985 cm^{-1} was assigned to bridge bonded carbonyl species on Pd couples on the edges of the metal particles, changed by the interaction with neighbouring Au atoms. These couples were oxidised in a lower extent (25% decrease) by the subsequent interactions with H_2 and O_2 and were involved in hydrogen dissociation during the reaction.

Quite different spectra were collected in the case of the catalyst in which firstly Pd and then gold were deposited (1Pd2Au, Figure 20c). No carbonyls on Pd^{2+} sites (band at 2160 cm^{-1}) were detected, because the chlorine atoms were removed during Au deposition in basic conditions. Au^0 sites (CO band at 2101 cm^{-1}) decorating the Pd edge couples (the band related to these CO bridge bonded species is totally missing) were observed. Conversely, the spectra collected on the PdAu catalyst (in which Pd and Au were simultaneously deposited) were quite similar to those obtained for 1Au2Pd sample (Figure 20d,b, respectively), with the exception of the carbonyls on Pd^0 edges (band at 2003 cm^{-1}), whose band was not affected by lateral interaction phenomena, indicating site isolation and the presence of small particles, according to HRTEM analysis.

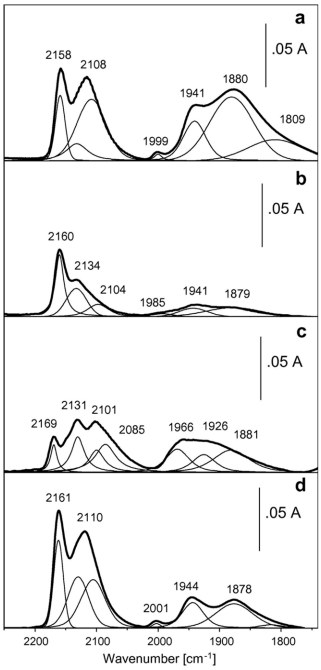

Figure 20. FTIR spectra of CO adsorbed at 180 K on Pd (**a**), 1Au2Pd (**b**), 1Pd2Au (**c**), and PdAu (**d**) after pre-treatment in H_2 and O_2 at r.t. (bold curves) and relative deconvolutions (fine curves). Reprinted from J. Catal., 268, F. Menegazzo, M. Signoretto, M. Manzoli, F. Boccuzzi, G. Cruciani, F. Pinna, G. Strukul, Influence of the preparation method on the morphological and composition properties of Pd–Au/ZrO_2 catalysts and their effect on the direct synthesis of hydrogen peroxide from hydrogen and oxygen, 122–130, Copyright (2009), with permission from Elsevier.

The authors suggested that the co-presence of the oxide layer activates molecular O_2 without dissociation, whereas the Pd^0 couples located on the edges dissociate hydrogen, explaining the improved productivity and selectivity towards H_2O_2.

3.4. Insights on the Exposed Sites and on the Properties of the Support

Very recently, Chung et al. developed the selective adsorption deposition method to prepare Pd/C catalysts with improved catalytic performance in the H_2O_2 direct synthesis [112]. The method consisted of (i) the selective adsorption of a cationic Pd precursor, $[Pd(NH_3)_4]^{2+}$, on a negatively-charged activated carbon surface, and (ii) conversion to Pd hydroxide in homogeneous phase in which the hydroxide ions were gradually produced upon urea decomposition. Following such procedure, it was possible to obtain ultra-small, monodispersed Pd nanoparticles with unprecedented and excellent catalytic activity. Indeed, the Pd/C#C1 catalyst gave a high initial H_2O_2 productivity of 8606 mmol $H_2O_2/(g_{Pd} \cdot h)$ and H_2 selectivity of 95.1% after 30 min reaction under safe and non-corrosive conditions. These results were 12 and 7.1 times higher, respectively, than those obtained for the catalyst prepared by conventional deposition-precipitation (Pd/C#A1).

DRIFT characterization, showed in Figure 21a, was carried out on the activated carbon treated with 1 wt% HNO_3 (green curve), 10 wt% HNO_3 (blue curve), and 10 wt% HNO_3/10 wt% H_2O_2 (red curve). The results firstly pointed out that the distribution of the oxygen groups on the activated carbon surface depends on the acid treatment conditions, and that large amounts of carboxyl groups were inserted on the surface of the activated carbon, according to titration, XPS, and TPD-mass experiments. More in detail, the C=O stretching band at 1780 cm^{-1} was assigned to carboxylic acid or to its anhydride form. Moreover, the peak around 1600 cm^{-1} was ascribed to the overlap of the polyaromatic C=C stretching bands of the highly conjugated carbonyl and/or quinone groups. Conversely, the broad band in the 1100–1450 cm^{-1} range was possibly due to the C=O stretching mode of carboxylic acid and of the lactone groups and/or to the O–H bending of phenol groups [113,114].

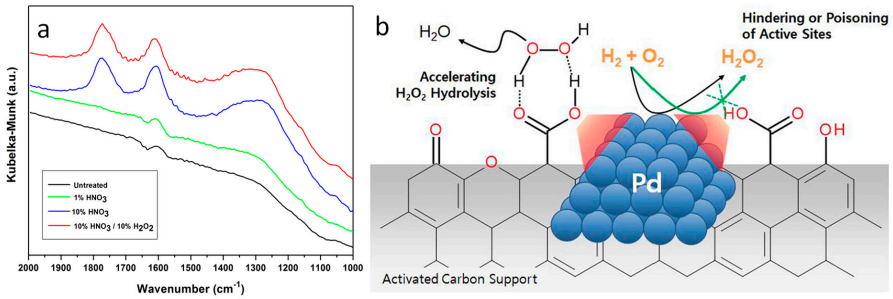

Figure 21. (**a**) DRIFTS-IR spectra or the surface-modified activated carbon. (**b**) Illustration of the unfavourable effect of carboxyl groups in accelerating H_2O_2 hydrolysis as well as hindering or poisoning the active metal sites. Reprinted from J. Catal., 365, S. Lee, H. Jeong, Y.-M. Chung, Direct synthesis of hydrogen peroxide over Pd/C catalyst prepared by selective adsorption deposition method, 125–137, Copyright (2018), with permission from Elsevier.

However, it was found that the carboxyl groups can negatively influence the catalytic activity, regardless of the preparation method. Indeed, the increase of the amount of carboxyl groups promoted H_2O_2 decomposition by hindering or poisoning the active sites. The authors suggested that despite H_2O_2 decomposition can be overcome in the presence of a strong electrolyte as H_2SO_4, carboxylic acid is a weak electrolyte, thus it does not efficiently suppress H–OOH dissociation, but preferentially foster H_2O_2 hydrolysis by forming hydrogen bonds, as described in Figure 21b.

A series of palladium catalysts supported on HZSM-5 with different Si/Al molar ratio (X = 15, 30, 75, 100, and 150) were prepared and tested in the hydrogen peroxide direct synthesis [67].

It was found that the electivity to H_2O_2 displayed a volcano-shaped curve with respect to the Si/Al molar ratio, whilst the hydrogen conversion showed no great difference. Thus, also the H_2O_2 yield showed a volcano-shaped curve and strictly depended on the Brønsted acidity/Lewis acidity (B/L) ratio of the Pd/HZSM-5-X catalysts.

In order to investigate the nature of the acid sites, in situ FT-IR spectroscopy of adsorbed pyridine was carried out, and the spectra collected on the Pd/HZSM-5-X catalysts are shown in Figure 22. The broad band at 1640 cm^{-1}, observed in all spectra was due to the bending vibration of O-H groups of H_2O adsorbed on the windows of the cell [115]. Upon pyridine adsorption, bands at 1440 and 1595 cm^{-1}, related to the presence of hydrogen bonded pyridine, at 1450, 1490, and 1580 cm^{-1} due to Lewis acid bound pyridine, and at 1490 and 1545 cm^{-1}, assigned to Brønsted acid bound pyridinium ion were observed on the Pd/HZSM-5- X catalysts [115–117].

Both Brønsted and Lewis acidity were quantified according to the procedure reported in the literature [118] by using the integrated molar extinction coefficients of 1.67 and 2.22 cm/μmol for Brønsted and Lewis acid sites, respectively. In particular, the quantities of Brønsted and Lewis acid sites were obtained from the integrated areas of the bands at 1545 and at 1450 cm^{-1}, according to Equations (4) and (5):

$$Bronsted\ acid\ site\ amount = \frac{IA(B) \times \pi \times R^2}{1.67 \times W} \quad (4)$$

$$Lewis\ acid\ site\ amount = \frac{IA(L) \times \pi \times R^2}{2.22 \times W} \quad (5)$$

where $IA(B)$ represents the integrated absorbance of Brønsted acid site (expressed in cm^{-1}), $IA(L)$ is the integrated absorbance of Lewis acid site (expressed in cm^{-1}), R is the inner radius of the sample cup (cm) and W is the weight of the catalyst (mg). The obtained B/L ratio displayed a volcano-shaped trend with respect to the Si/Al molar ratio, and the Pd/HZSM-5-30 catalyst had the highest B/L ratio. In particular, Brønsted acid sites in HZSM-5 are due to the presence of bridging hydroxyl group in Si–OH–Al moieties [119,120]. Conversely, the Lewis acid sites are the Al in the hydroxoaluminum complex [119]. Hence, the authors come to the conclusion that the B/L ratio was decreased by

increasing the totality of Lewis acid sites, in consequence of the increase of the population of the hydroxoaluminum complex upon incorporation of a large Al amount into the HZSM-5 framework.

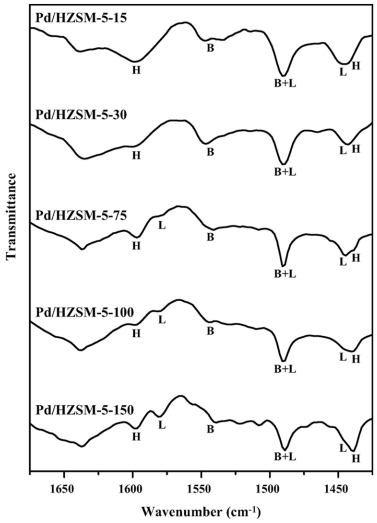

Figure 22. FT-IR spectra of pyridine adsorbed on Pd/HZSM-5-X (X = 15, 30, 75, 100, and 150) catalysts. H: hydrogen bonded pyridine; L: Lewis acid bound pyridine; B: Brønsted acid bound pyridinium ion. Reprinted from J. Molecul. Catal. A: Chemical, 363, S. Park, J. Lee, J. H. Song, T. J. Kim, Y.-M. Chung, S.-H. Oh, I. K. Song, Direct synthesis of hydrogen peroxide from hydrogen and oxygen over Pd/HZSM-5 catalysts: Effect of Brønsted acidity, 230–236, Copyright (2012), with permission from Elsevier.

Interestingly, it was found that the H_2O_2 yield increased by augmenting the B/L ratio, which points out the key role played by Brønsted acid sites of the Pd/HZSM-5-X catalysts. Indeed, the catalyst with the highest Brønsted acidity (Pd/HZSM-5-30) gave the largest yield. A correlation between the H_2O_2 yield and the B/L ratio of the Pd/HZSM-5-X catalysts was shown (see Figure 23a), unambiguously showing that the yield was intimately linked to the B/L ratio. Moreover, the yield increased with the Brønsted acidity measured by ammonia temperature-programmed desorption (TPD) measurements (Figure 23b). These results were consistent with the increase in H_2O_2 selectivity observed by the addition of acid additives [1,61].

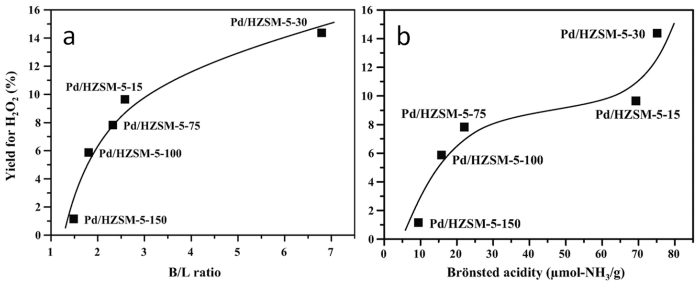

Figure 23. (**a**) Correlation between yield for hydrogen peroxide over Pd/HZSM-5-X (X = 15, 30, 75, 100, and 150) catalysts and B/L ratio of the catalysts. (**b**) Correlation between yield for hydrogen peroxide over Pd/HZSM-5-*X* (*X* = 15, 30, 75, 100, and 150) catalysts and Brønsted acidity of the catalysts. Adapted from J. Molecul. Catal. A: Chemical, 363, S. Park, J. Lee, J. H. Song, T. J. Kim, Y.-M. Chung, S.-H. Oh, I. K. Song, Direct synthesis of hydrogen peroxide from hydrogen and oxygen over Pd/HZSM-5 catalysts: Effect of Brønsted acidity, 230–236, Copyright (2012), with permission from Elsevier.

Au-Pd bimetallic catalysts are very efficient in the H_2O_2 direct synthesis process, in particular when supported on acidic supports. Indeed, the use of acidic supports promotes the hydrogen

peroxide stabilization and can also inhibit the hydrogenation and decomposition reactions. The preparation and testing of Au-Pd catalysts supported on insoluble heteropolyacids were reported by Hutchings et al. [65]. Ions such as Cs^+, Rb^+, K^+, and Ag^+ counterbalance the charge of the heteropolyacids supports, and the catalyst were prepared by ion exchange and impregnation methods. The FTIR spectra collected on the bare heteropolyacids containing different counter ions are reported in Figure 24a. The typical features of the Keggin structure of Cs substituted phosphotungstic acid were observed in all spectra [121].

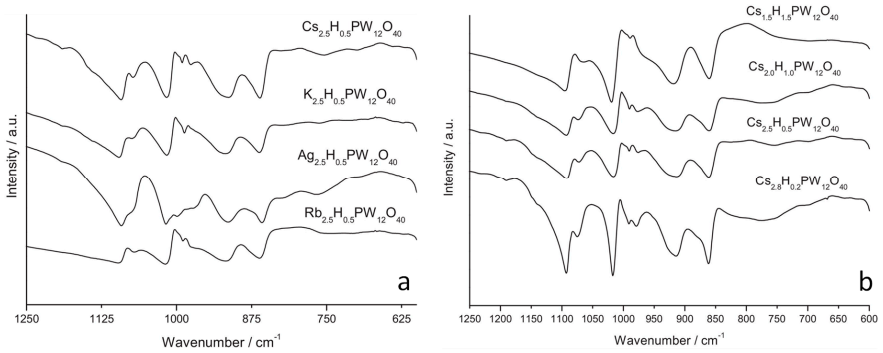

Figure 24. (**a**) FT-IR spectra of heteropolyacid support materials made by incorporating various metal ions. (**b**) FT-IR spectra of heteropolyacid support materials made by incorporating various about of Cs ions. Reprinted from Catal. Today, 248, S. J. Freakley, R. J. Lewis, D. J. Morgan, J. K. Edwards, G. J. Hutchings, Direct synthesis of hydrogen peroxide using Au–Pd supported and ion-exchanged heteropolyacids precipitated with various metal ions, 10–17, Copyright (2015), with permission from Elsevier.

More in detail, the vibrational bands for the Keggin structure were detected at 1090 cm^{-1} that is due to ν_{as}(P-O) vibration, at 1016 cm^{-1}, assigned to terminal ν_{as}(W = O vibration, and 912 and 863 cm^{-1}, due to ν_{as}(W-O-W) vibrations. In some cases, bands at 1710 cm^{-1} distinctive of protonated $H_5O_2^+$ clusters were observed, but the spectra were collected in air and therefore these (O-H) vibrations cannot be solely ascribed to the heteropolyacid structure and the intensity of this absorption band cannot be taken as a measure of the acidity of the catalysts. Moreover, the P-O stretching mode was observed in all samples upon Cs^+ substitution, pointing out that the substitution of Cs^+ for H^+ did not induce strain on the P-O_4 tetrahedra within the structure. The incorporation of Au and Pd by impregnation or by ion exchange did not originate any change or new band in the spectra, possibly because of the very small amounts of Au and Pd that were introduced gave rise to signals under the detection limit. The Keggin structure was maintained after calcination of the catalysts and also after the incorporation of different amounts of Cs^+ (Figure 24b), according to the XRD results.

The H_2O_2 productivity reached by $Pd_{0.075}Au_{0.05}Cs_{2.5}H_{0.5}W_{12}O_{40}$ was much higher than that obtained by the most active conventional catalyst 2.5% Au/2.5% Pd/C (2% HNO_3), but the H_2O_2 degradation rate was comparable. Despite the notably high degradation rates, the catalysts containing Cs^+ and Rb^+ (Au/2.5% Pd/$Rb_{2.5}H_{0.5}PW_{12}O_{40}$ and 2.5% Au/2.5% Pd/$Cs_{2.5}H_{0.5}PW_{12}O_{40}$) and prepared by ion exchange were remarkably more active (an order of magnitude higher) than the conventional catalyst under reaction conditions prescribed by potential applications (water as a solvent and ambient temperature). Based on environmental and economic considerations, the authors suggested that these catalysts could be the starting point for the design of more efficient catalysts for the H_2O_2 direct synthesis.

Monometallic Pd and bimetallic PdAu catalysts supported on SBA15 and SiO_2 were synthesized and tested in the H_2O_2 direct synthesis by using a batch autoclave (at 10 °C and 17.5 bar) without the addition of halides and acids [122]. SBA15-supported catalysts displayed better performance with respect to those supported on SiO_2 (Si), due to the possibility to regulate the dispersion in the 5–7 nm range, as well as the stability of the nanoparticles. Interestingly, despite bromine is a well-known a

promoter of the H_2O_2 direct synthesis, a decrease in both productivity and selectivity was observed upon bromopropylsilane addition during the grafting process, as a consequence of larger size poor stability of the metal nanoparticles, as revealed by TEM images. However, a synergistic effect between Pd and Au was highlighted either in the presence or in the absence of bromopropylsilane grafting on the catalyst surface. Moreover, SBA15 was modified by the addition of Al, CeO_2, and Ti to investigate the effect of the surface properties of the support on the dispersion of the metal phase and on the catalytic activity. According to Table 2, the catalyst in which Al was incorporated (PdAu/Al-SBA15) displayed higher productivity and selectivity. On the contrary, no improvement of the H_2O_2 yields was observed by adding Ti or CeO_2.

Table 2. H_2O_2 synthesis with SBA15 supported catalysts: acidity, H_2 conversion after 15 min of reaction, productivity and selectivity (after 15 min of reaction and at complete H_2 conversion). Reprinted by permission from Springer Nature: Springer Nature, Topics in Catalysis, 56, 540–549, Reactivity Aspects of SBA15-Based Doped Supported Catalysts: H_2O_2 Direct Synthesis and Disproportionation Reactions, N. Gemo, P. Biasi, P. Canu, F. Menegazzo, F. Pinna, A. Samikannu, K. Kordás, T. O. Salmi, J.-P. Mikkola, Copyright (2013).

Catalyst	Productivity H_2O_2 (mol H_2O_2/mol$_{metal}$ h)		Selectivity (%)		H_2 Conversion @ 15 min	Complete H_2 Conversion	Acidity (μmol/g)	
	@ 15 min	@ Complete H_2 Conversion	@ 15 min	@ Complete H_2 Conversion	(%)	(min)	Lewis	Brønsted
Pd/SBA15	359	311	20	20	99	20	-	-
PdAu/SBA15	634	326	28	24	65	41	-	-
Br-Pd/SBA15	39	-	-	-	-	-	-	-
Br-PdAu/SBA15	192	-	24	-	13	-	-	-
PdAu-Br/SBA15	0	0	0	0	-	-	-	-
Pd/Si	850	234	17	15	51	85	-	-
PdAu/Si	183	77	8	8	77	57	-	-
PdAu/CeO_2-SBA15	399	314	16	14	48	34	39	0
PdAu/Ti-SBA15	538	463	13	12	77	18	16	0
PdAu/Al-SBA15	870	422	30	24	67	37	22	8
Br-PdAu/Al-SBA15	76	-	20	-	11	-	9	0

Conditions: T = 10 °C, P = 17.5 bar.

The improved performance of PdAu/Al–SBA15 was ascribed to an increased amount of Brønsted acid sites as reveled by FT-IR spectroscopy of adsorbed pyridine. In addition, the presence of Brønsted and/or Lewis acid sites was revealed in the modified SBA15 supports. The spectroscopic experiments were carried out according to the reported procedure [118]. The spectra were collected at different temperatures (250, 350, and 450 °C) and the bands related to adsorbed pyridine were detected only at 250 °C. Measured acid sites concentrations are reported in Table 1 (entries 8–11). The amounts of Lewis and Brønsted acid sites were estimated on areas of the bands observed at 1450 and 1545 cm^{-1}, by assuming 1.67 cm/μmol (Brønsted sites) and 2.22 cm/μmol (Lewis sites) integrated molar extinction coefficients. In addition, these analyses pointed out the presence of Brønsted and/or Lewis acid sites in the modified SBA15 supports. The authors showed that the H_2O_2 hydrogenation was overcome when the peroxide is surrounded by protons, i.e., the Brønsted acid sites [61,68]. Therefore, the H_2O_2 productivity can be enhanced by increasing the Brønsted acidity by Al insertion.

4. Final Remarks and Open Issues

FTIR spectroscopy, either in transmission or in DRIFT mode, was shown to be a flexible technique which can be easily adapted to investigate the large variety of catalytic systems described here in order to establish catalyst structure-activity relationships in direct H_2O_2 synthesis.

Despite being one of the first spectroscopic techniques employed for catalyst characterization, it can be considered as one of the most effective to obtain detailed chemical information on systems with continuously increasing complexity. Indeed, FTIR spectroscopy allowed, with no particular

effort (and with acceptable instrumentation costs), to shed light on the nature and on the properties of the active sites exposed at the surface of the Pd nanoparticles, which are the most active, as well as the most commonly investigated, catalyst for hydrogen peroxide direct synthesis. The selectivity of such systems is improved by the addition of a second metal in order to inhibit the sites that are active for dissociative oxygen activation. Studies dealing with the addition of several heteroatoms to the active palladium phase have demonstrated that accurate analysis of the spectra of adsorbed probes (mainly CO) collected in well-controlled experimental conditions, allows for obtaining deep and precious insights on Pd site isolation and electronic effects.

Many papers investigated, in detail, the nature of exposed active metal sites, however, only a minority tried to monitor by IR spectroscopy the reactivity of the exposed metal sites towards the molecular hydrogen and oxygen reactants, and to obtain information regarding the relative coverages of the reactive species present on the metal nanoparticles during catalysis. Additionally, FTIR characterization provided insights on the exposed sites of the employed supports and on their properties. Opportune probe molecules were used to measure the acidity and to quantify the Brønsted and the Lewis sites.

Nevertheless, FTIR absorption spectroscopy needs to be combined with many other techniques, such as XAS, especially with in situ or operando studies during direct H_2O_2 synthesis, to correlate the electronic and structural states of Pd with the catalytic performance, as exemplified in Figure 25.

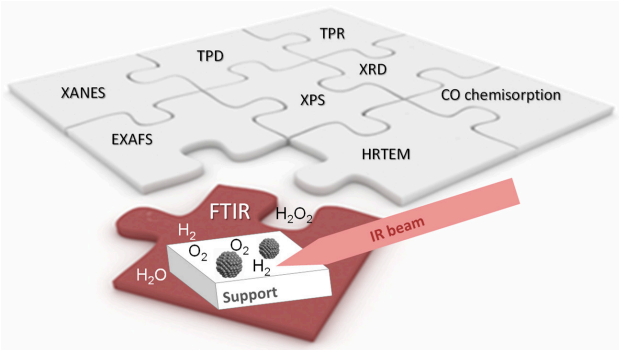

Figure 25. Role of the FTIR spectroscopy in catalyst characterisation.

Therefore, FTIR characterization contributed significantly to the development of a rational design for new catalysts and of the optimization of process parameters for H_2O_2 direct synthesis. However, there are many paths to be covered in the use of FTIR absorption spectroscopy for future studies in H_2O_2 direct synthesis. Some possible directions can be tentatively proposed here.

In situ studies performed at low temperature could potentially be useful to investigate the saturation of the metal active sites with O2* and OOH* species during the reaction in alcohol solvents [3,90]. In this frame, IR spectroscopy can detect peroxides or superoxides that would support the effective presence of these intermediates.

The addition halides to prevent O_2 dissociation can result in the presence of dense adlayers [62], the effects of the presence of halides on the metal sites have not been investigated yet by IR spectroscopy.

Restructuring (and degradation [13]) phenomena occurring on the metal nanoparticles under reaction conditions could be monitored using a combined XAFS/DRIFTS or FTIR transmission approach, as proposed by Gibson et al. for AuPd bimetallic catalysts during CO oxidation [123].

At present, isotopic studies are underestimated despite their ability to identify distinct active sites and to probe the kinetics and reversibility of specific steps [45].

Acknowledgments: This work was supported by the University of Turin (Progetti Ricerca Locale 2018).

Conflicts of Interest: Maela Manzoli declares no conflict of interest.

References

1. Campos-Martin, J.M.; Blanco-Brieva, G.; Fierro, J.L.G. Hydrogen Peroxide Synthesis: An Outlook beyond the Anthraquinone Process. *Angew. Chem. Int. Ed.* **2006**, *45*, 6962–6984. [CrossRef] [PubMed]
2. Riedl, H.-J.; Pfleiderer, G. Production of Hydrogen Peroxide. U.S. Patent No. 2215883, 24 September 1940.
3. Wilson, N.M.; Flaherty, D.W. Mechanism for the Direct Synthesis of H_2O_2 on Pd Clusters: Heterolytic Reaction Pathways at the Liquid−Solid Interface. *J. Am. Chem. Soc.* **2015**, *138*, 574–586. [CrossRef] [PubMed]
4. Flaherty, D.W. Direct Synthesis of H_2O_2 from H_2 and O_2 on Pd Catalysts: Current Understanding, Outstanding Questions, and Research Needs Motivation and Challenges for Direct Synthesis of H_2O_2. *ACS Catal.* **2018**, *8*, 1520–1527. [CrossRef]
5. Wilson, N.M.; Bregante, D.T.; Priyadarshini, P.; Flaherty, D.W. Production and use of H_2O_2 for atom-efficient functionalization of hydrocarbons and small molecules. In *Catalysis*; Spivey, J., Han, Y.-F., Eds.; Royal Society of Chemistry: London, UK, 2017; Volume 29, pp. 122–212.
6. Yang, S.; Verdaguer-Casadevall, A.; Arnarson, L.; Silvioli, L.; Frydendal, R.; Rossmeisl, J.; Chorkendorff, I.L.; Stephens, I.E. Toward the Decentralized Electrochemical Production of H_2O_2: A Focus on the Catalysis. *ACS Catal.* **2018**, *8*, 4064–4081. [CrossRef]
7. Gosser, L.W. Catalytic Process for Making H_2O_2 from Hydrogen and Oxygen. U.S. Patent No. 4681751, 21 July 1987.
8. Gosser, L.W.; Schwartz, J.-A.T. Catalytic Process for Making Hydrogen Peroxide from Hydrogen and Oxygen Employing a Bromide Promoter. U.S. Patent No. 4772458, 20 September 1988.
9. Colery, J.-C.; Van Weynbergh, J.; Schoebrechts, J.-P. Direct Synthesis of Hydrogen Peroxide by Heterogeneous Catalysis, Catalyst for the Said Synthesis and Method of Preparation of the Said Catalyst. U.S. Patent No. 5447706, 5 September 1995.
10. Bertsch-Frank, B.; Balduf, T.; Becker-Balfanz, C.; Hemme, I.; Rollmann, J.; Schutte, R.; Wildner, W. Process for Producing Hydrogen Peroxide by Direct Synthesis. U.S. Patent No. 6,387,346B1, 14 May 2002.
11. Vanden Bussche, K.M.; Abdo, S.F.; Oroskar, A.R. Process for Mixing and Reacting Two or More Fluids. U.S. Patent No. 6713036 B1, 30 March 2004.
12. Samanta, C.; Choudhary, V.R. Direct formation of H_2O_2 from H_2 and O_2 and decomposition/hydrogenation of H_2O_2 in aqueous acidic reaction medium over halide-containing Pd/SiO_2 catalytic system. *Catal. Commun.* **2007**, *8*, 2222–2228. [CrossRef]
13. Pizzutilo, E.; Freakley, S.J.; Cherevko, S.; Venkatesan, S.; Hutchings, G.J.; Liebscher, C.H.; Dehm, G.; Mayrhofer, K.J.J. Gold−Palladium Bimetallic Catalyst Stability: Consequences for Hydrogen Peroxide Selectivity. *ACS Catal.* **2017**, *7*, 5699–5705. [CrossRef]
14. Biasi, P.; Menegazzo, F.; Pinna, F.; Eränen, K.; Salmi, T.O.; Canu, P. Continuous H_2O_2 direct synthesis over PdAu catalysts. *Chem. Eng. J.* **2011**, *176–177*, 172–177. [CrossRef]
15. Verdaguer-Casadevall, A.; Deiana, D.; Karamad, M.; Siahrostami, S.; Malacrida, P.; Hansen, T.W.; Rossmeisl, J.; Chorkendorff, I.; Stephens, I.E.L. Trends in the Electrochemical Synthesis of H_2O_2: Enhancing Activity and Selectivity by Electrocatalytic Site Engineering. *Nano Lett.* **2014**, *14*, 1603–1608. [CrossRef]
16. Lunsford, J.H. The direct formation of H_2O_2 from H_2 and O_2 over palladium catalysts. *J. Catal.* **2003**, *216*, 455–460. [CrossRef]
17. Yi, Y.; Wang, L.; Li, G.; Guo, H. A review on research progress in the direct synthesis of hydrogen peroxide from hydrogen and oxygen: Noble-metal catalytic method, fuel-cell method and plasma method. *Catal. Sci. Technol.* **2016**, *6*, 1593–1610. [CrossRef]
18. Choudhary, V.R.; Samanta, C. Role of chloride or bromide anions and protons for promoting the selective oxidation of H_2 by O_2 to H_2O_2 over supported Pd catalysts in an aqueous medium. *J. Catal.* **2006**, *238*, 28–38. [CrossRef]
19. Choudhary, V.R.; Samanta, C.; Choudhary, T.V. Direct oxidation of H_2 to H_2O_2 over Pd-based catalysts: Influence of oxidation state, support and metal additives. *Appl. Catal. A Gen.* **2006**, *308*, 128–133. [CrossRef]
20. Burch, R.; Ellis, P.R. An investigation of alternative catalytic approaches for the direct synthesis of hydrogen peroxide from hydrogen and oxygen. *Appl. Catal. B Environ.* **2003**, *42*, 203–211. [CrossRef]
21. Edwards, J.K.; Solsona, B.; Ntainjua, E.; Carley, A.F.; Herzing, A.A.; Kiely, C.J.; Hutchings, G.J. Switching Off Hydrogen Peroxide Hydrogenation in the Direct Synthesis Process. *Science* **2009**, *323*, 1037–1041. [CrossRef]

22. Akram, A.; Freakley, S.J.; Reece, C.; Piccinini, M.; Shaw, G.; Edwards, J.K.; Desmedt, F.; Miquel, P.; Seuna, E.; Willock, D.J.; et al. Gas phase stabiliser-free production of hydrogen peroxide using supported gold–palladium catalysts. *Chem. Sci.* **2016**, *7*, 5833–5837. [CrossRef] [PubMed]
23. Crole, D.A.; Freakley, S.J.; Edwards, J.K.; Hutchings, G.J. Direct synthesis of hydrogen peroxide in water at ambient temperature. *Proc. R. Soc. A Math. Phys. Eng. Sci.* **2016**, *472*, 20160156. [CrossRef] [PubMed]
24. Park, S.; Baeck, S.-H.; Kim, T.J.; Chung, Y.-M.; Oh, S.-H.; Song, I.K. Direct synthesis of hydrogen peroxide from hydrogen and oxygen over palladium catalyst supported on SO_3H-functionalized mesoporous silica. *J. Mol. Catal. A Chem.* **2010**, *319*, 98–107. [CrossRef]
25. Edwards, J.K.; Freakley, S.J.; Carley, A.F.; Kiely, C.J.; Hutchings, G.J. Strategies for Designing Supported Gold-Palladium Bimetallic Catalysts for the Direct Synthesis of Hydrogen Peroxide. *Acc. Chem. Res.* **2013**, *47*, 845–854. [CrossRef]
26. Solsona, B.E.; Edwards, J.K.; Landon, P.; Carley, A.F.; Herzing, A.; Kiely, C.J.; Hutchings, G.J. Direct Synthesis of Hydrogen Peroxide from H_2 and O_2 Using Al_2O_3 Supported Au–Pd Catalysts. *Chem. Mater.* **2006**, *18*, 2689–2695. [CrossRef]
27. Edwards, J.K.; Solsona, B.E.; Landon, P.; Carley, A.F.; Herzing, A.; Kiely, C.J.; Hutchings, G.J. Direct synthesis of hydrogen peroxide from H_2 and O_2 using TiO_2-supported Au–Pd catalysts. *J. Catal.* **2005**, *236*, 69–79. [CrossRef]
28. Jeong, H.E.; Kim, S.; Seo, M.; Lee, D.-W.; Lee, K.-Y. Catalytic activity of Pd octahedrons/SiO_2 for the direct synthesis of hydrogen peroxide from hydrogen and oxygen. *J. Mol. Catal. A Chem.* **2016**, *420*, 88–95. [CrossRef]
29. Selinsek, M.; Deschner, B.J.; Doronkin, D.E.; Sheppard, T.L.; Grunwaldt, J.-D.; Dittmeyer, R. Revealing the Structure and Mechanism of Palladium during Direct Synthesis of Hydrogen Peroxide in Continuous Flow Using Operando Spectroscopy. *ACS Catal.* **2018**, *8*, 2546–2557. [CrossRef]
30. Biasi, P.; Sterchele, S.; Bizzotto, F.; Manzoli, M.; Lindholm, S.; Ek, P.; Bobacka, J.; Mikkola, J.-P.; Salmi, T. Application of the Catalyst Wet Pretreatment Method (CWPM) for catalytic direct synthesis of H_2O_2. *Catal. Today* **2015**, *246*, 207–215. [CrossRef]
31. Menegazzo, F.; Signoretto, M.; Frison, G.; Pinna, F.; Strukul, G.; Manzoli, M.; Boccuzzi, F. When high metal dispersion has a detrimental effect: Hydrogen peroxide direct synthesis under very mild and nonexplosive conditions catalyzed by Pd supported on silica. *J. Catal.* **2012**, *290*. [CrossRef]
32. Abate, S.; Arrigo, R.; Schuster, M.E.; Perathoner, S.; Centi, G.; Villa, A.; Su, D.; Schlögl, R. Pd nanoparticles supported on N-doped nanocarbon for the direct synthesis of H_2O_2 from H_2 and O_2. *Catal. Today* **2010**, *157*, 280–285. [CrossRef]
33. Kim, J.; Chung, Y.-M.; Kang, S.-M.; Choi, C.-H.; Kim, B.-Y.; Kwon, Y.-T.; Jin Kim, T.; Oh, S.-H.; Lee, C.-S. Palladium Nanocatalysts Immobilized on Functionalized Resin for the Direct Synthesis of Hydrogen Peroxide from Hydrogen and Oxygen. *ACS Catal.* **2012**, *2*, 1042–1048. [CrossRef]
34. Seo, M.-G.; Lee, D.-W.; Han, S.S.; Lee, K.-Y. Direct Synthesis of Hydrogen Peroxide from Hydrogen and Oxygen over Mesoporous Silica-Shell-Coated, Palladium-Nanocrystal-Grafted SiO_2 Nanobeads. *ACS Catal.* **2017**, *7*, 3039–3048. [CrossRef]
35. Gervasini, A.; Carniti, P.; Frédé, F.; Desmedt, F.; Miquel, P. Liquid Phase Direct Synthesis of H_2O_2: Activity and Selectivity of Pd-Dispersed Phase on Acidic Niobia-Silica Supports. *ACS Catal.* **2017**, *7*, 3039–3048. [CrossRef]
36. Krishnankutty, N.; Li, J.; Albert Vannice, M. The effect of Pd precursor and pretreatment on the adsorption and absorption behavior of supported Pd catalysts. *Appl. Catal. A Gen.* **1998**, *173*, 137–144. [CrossRef]
37. Seo, M.; Kim, S.; Jeong, H.E.; Lee, D.-W.; Lee, K.-Y. A yolk–shell structured Pd@void@ZrO_2 catalyst for direct synthesis of hydrogen peroxide from hydrogen and oxygen. *J. Mol. Catal. A Chem.* **2016**, *413*, 1–6. [CrossRef]
38. Yook, S.; Kwon, H.C.; Kim, Y.-G.; Choi, W.; Choi, M. Significant Roles of Carbon Pore and Surface Structure in AuPd/C Catalyst for Achieving High Chemoselectivity in Direct Hydrogen Peroxide Synthesis. *ACS Sustain. Chem. Eng.* **2016**, *5*, 1208–1216. [CrossRef]
39. Menegazzo, F.; Signoretto, M.; Manzoli, M.; Boccuzzi, F.; Cruciani, G.; Pinna, F.; Strukul, G. Influence of the preparation method on the morphological and composition properties of Pd–Au/ZrO_2 catalysts and their effect on the direct synthesis of hydrogen peroxide from hydrogen and oxygen. *J. Catal.* **2009**, *268*, 122–130. [CrossRef]

40. Menegazzo, F.; Manzoli, M.; Signoretto, M.; Pinna, F.; Strukul, G. H_2O_2 direct synthesis under mild conditions on Pd-Au samples: Effect of the morphology and of the composition of the metallic phase. *Catal. Today* **2014**, *248*, 18–27. [CrossRef]
41. Edwards, J.K.; Hutchings, G.J. Palladium and Gold-Palladium Catalysts for the Direct Synthesis of Hydrogen Peroxide. *Angew. Chem. Int. Ed.* **2008**, *47*, 9192–9198. [CrossRef] [PubMed]
42. Xu, H.; Cheng, D.; Gao, Y. Design of High-Performance Pd-Based Alloy Nanocatalysts for Direct Synthesis of H_2O_2. *ACS Catal.* **2017**, *7*, 2164–2170. [CrossRef]
43. García, T.; Agouram, S.; Dejoz, A.; Sánchez-Royo, J.F.; Torrente-Murciano, L.; Solsona, B. Enhanced H_2O_2 production over Au-rich bimetallic Au–Pd nanoparticles on ordered mesoporous carbons. *Catal. Today* **2015**, *248*, 48–57. [CrossRef]
44. Arrigo, R.; Schuster, M.E.; Abate, S.; Wrabetz, S.; Amakawa, K.; Teschner, D.; Freni, M.; Centi, G.; Perathoner, S.; Hävecker, M.; Schlögl, R. Dynamics of Palladium on Nanocarbon in the Direct Synthesis of H_2O_2. *ChemSusChem* **2014**, *7*, 179–194. [CrossRef]
45. Wilson, N.M.; Pan, Y.-T.; Shao, Y.-T.; Zuo, J.-M.; Yang, H.; Flaherty, D.W. Direct Synthesis of H_2O_2 on AgPt Octahedra: The Importance of Ag–Pt Coordination for High H_2O_2 Selectivity. *ACS Catal.* **2018**, *8*, 2880–2889. [CrossRef]
46. Prati, L.; Villa, A.; Campisi, S.; Vindigni, F.; Manzoli, M.; Dimitratos, N. Support acid-base properties as a tool for directing selectivity in the Au-Pt catalyzed base-free glycerol oxidation. In Proceedings of the Engineering Sciences and Fundamentals 2013—Core Programming Area at the 2013 AIChE Annual Meeting: Global Challenges for Engineering a Sustainable Future, San Francisco, CA, USA, 3–8 November 2013; Volume 2.
47. Bernardotto, G.; Menegazzo, F.; Pinna, F.; Signoretto, M.; Cruciani, G.; Strukul, G. New Pd–Pt and Pd–Au catalysts for an efficient synthesis of H_2O_2 from H_2 and O_2 under very mild conditions. *Appl. Catal. A Gen.* **2009**, *358*, 129–135. [CrossRef]
48. Liu, Q.; Bauer, J.C.; Schaak, R.E.; Lunsford, J.H. Direct synthesis of H_2O_2 from H_2 and O_2 over Pd–Pt/SiO2 bimetallic catalysts in a H2SO4/ethanol system. *Appl. Catal. A Gen.* **2008**, *339*, 130–136. [CrossRef]
49. Freakley, S.J.; He, Q.; Harrhy, J.H.; Lu, L.; Crole, D.A.; Morgan, D.J.; Ntainjua, E.N.; Edwards, J.K.; Carley, A.F.; Borisevich, A.Y.; et al. Palladium-tin catalysts for the direct synthesis of H_2O_2 with high selectivity. *Science* **2016**, *351*, 965–968. [CrossRef] [PubMed]
50. Li, F.; Shao, Q.; Hu, M.; Chen, Y.; Huang, X. Hollow Pd−Sn Nanocrystals for Efficient Direct H_2O_2 Synthesis: The Critical Role of Sn on Structure Evolution and Catalytic Performance. *ACS Catal.* **2018**, *8*, 3418–3423. [CrossRef]
51. Maity, S.; Eswaramoorthy, M. Ni–Pd bimetallic catalysts for the direct synthesis of H_2O_2—Unusual enhancement of Pd activity in the presence of Ni. *J. Mater. Chem. A* **2016**, *4*, 3233–3237. [CrossRef]
52. Tian, P.; Xu, X.; Ao, C.; Ding, D.; Li, W.; Si, R.; Tu, W.; Xu, J.; Han, Y.-F. Direct and Selective Synthesis of Hydrogen Peroxide over Palladium-Tellurium Catalysts at Ambient Pressure. *ChemSusChem* **2017**, *10*, 3342–3346. [CrossRef]
53. Childers, D.J.; Schweitzer, N.M.; Shahari, S.M.K.; Rioux, R.M.; Miller, J.T.; Meyer, R.J. Modifying structure-sensitive reactions by addition of Zn to Pd. *J. Catal.* **2014**, *318*, 75–84. [CrossRef]
54. Wang, S.; Gao, K.; Li, W.; Zhang, J. Effect of Zn addition on the direct synthesis of hydrogen peroxide over supported palladium catalysts. *Appl. Catal. A Gen.* **2017**, *531*, 89–95. [CrossRef]
55. Li, G.; Edwards, J.; Carley, A.F.; Hutchings, G.J. Direct synthesis of hydrogen peroxide from H_2 and O_2 and in situ oxidation using zeolite-supported catalysts. *Catal. Commun.* **2007**, *8*, 247–250. [CrossRef]
56. Hu, B.; Deng, W.; Li, R.; Zhang, Q.; Wang, Y.; Delplanque-Janssens, F.; Paul, D.; Desmedt, F.; Miquel, P. Carbon-supported palladium catalysts for the direct synthesis of hydrogen peroxide from hydrogen and oxygen. *J. Catal.* **2014**, *319*, 15–26. [CrossRef]
57. Tian, P.; Ouyang, L.; Xu, X.; Ao, C.; Xu, X.; Si, R.; Shen, X.; Lin, M.; Xu, J.; Han, Y.-F. The origin of palladium particle size effects in the direct synthesis of H_2O_2: Is smaller better? *J. Catal.* **2017**, *349*, 30–40. [CrossRef]
58. Han, Y.-F.; Lunsford, J.H. Direct formation of H_2O_2 from H_2 and O_2 over a Pd/SiO_2 catalyst: The roles of the acid and the liquid phase. *J. Catal.* **2005**, *230*, 313–316. [CrossRef]

59. Ouyang, L.; Tian, P.; Da, G.; Xu, X.-C.; Ao, C.; Chen, T.; Si, R.; Xu, J.; Han, Y.-F. The origin of active sites for direct synthesis of H_2O_2 on Pd/TiO_2 catalysts: Interfaces of Pd and PdO domains. *J. Catal.* **2015**, *321*, 70–80. [CrossRef]
60. Lari, G.M.; Puértolas, B.; Shahrokhi, M.; López, N.; Pérez-Ramírez, J. Hybrid Palladium Nanoparticles for Direct Hydrogen Peroxide Synthesis: The Key Role of the Ligand. *Angew. Chem. Int. Ed.* **2017**, *56*, 1775–1779. [CrossRef] [PubMed]
61. Samanta, C. Direct synthesis of hydrogen peroxide from hydrogen and oxygen: An overview of recent developments in the process. *Appl. Catal. A Gen.* **2008**, *350*, 133–149. [CrossRef]
62. Chinta, S.; Lunsford, J.H. A mechanistic study of H_2O_2 and H_2O formation from H_2 and O_2 catalyzed by palladium in an aqueous medium. *J. Catal.* **2004**, *225*, 249–255. [CrossRef]
63. Melada, S.; Rioda, R.; Menegazzo, F.; Pinna, F.; Strukul, G. Direct synthesis of hydrogen peroxide on zirconia-supported catalysts under mild conditions. *J. Catal.* **2006**, *239*, 422–430. [CrossRef]
64. Park, S.; Lee, S.H.; Song, S.H.; Park, D.R.; Baeck, S.-H.; Kim, T.J.; Chung, Y.-M.; Oh, S.-H.; Song, I.K. Direct synthesis of hydrogen peroxide from hydrogen and oxygen over palladium-exchanged insoluble heteropolyacid catalysts. *Catal. Commun.* **2009**, *10*, 391–394. [CrossRef]
65. Freakley, S.J.; Lewis, R.J.; Morgan, D.J.; Edwards, J.K.; Hutchings, G.J. Direct synthesis of hydrogen peroxide using Au–Pd supported and ion-exchanged heteropolyacids precipitated with various metal ions. *Catal. Today* **2015**, *248*, 10–17. [CrossRef]
66. Park, S.; Park, D.R.; Choi, J.H.; Kim, T.J.; Chung, Y.-M.; Oh, S.-H.; Song, I.K. Direct synthesis of hydrogen peroxide from hydrogen and oxygen over palladium catalyst supported on $H_3PW_{12}O_{40}$-incorporated MCF silica. *J. Mol. Catal. A Chem.* **2011**, *336*, 78–86. [CrossRef]
67. Park, S.; Lee, J.; Song, J.H.; Kim, T.J.; Chung, Y.-M.; Oh, S.-H.; Song, I.K. Direct synthesis of hydrogen peroxide from hydrogen and oxygen over Pd/HZSM-5 catalysts: Effect of Brönsted acidity. *J. Mol. Catal. A Chem.* **2012**, *363–364*, 230–236. [CrossRef]
68. Park, S.; Choi, J.H.; Kim, T.J.; Chung, Y.-M.; Oh, S.-H.; Song, I.K. Direct synthesis of hydrogen peroxide from hydrogen and oxygen over $Pd/CsXH_3-XPW_{12}O_{40}$/MCF (X = 1.7, 2.0, 2.2, 2.5, and 2.7) catalysts. *J. Mol. Catal. A Chem.* **2012**, *353*, 37–43. [CrossRef]
69. Park, S.; Park, D.R.; Choi, J.H.; Kim, T.J.; Chung, Y.-M.; Oh, S.-H.; Song, I.K. Direct synthesis of hydrogen peroxide from hydrogen and oxygen over insoluble $Cs_{2.5}H_{0.5}PW_{12}O_{40}$ heteropolyacid supported on Pd/MCF. *J. Mol. Catal. A Chem.* **2010**, *332*, 76–83. [CrossRef]
70. Lewis, R.J.; Edwards, J.K.; Freakley, S.J.; Hutchings, G.J. Solid Acid Additives as Recoverable Promoters for the Direct Synthesis of Hydrogen Peroxide. *Ind. Eng. Chem. Res.* **2017**, *56*, 13287–13293. [CrossRef]
71. Zaera, F. New advances in the use of infrared absorption spectroscopy for the characterization of heterogeneous catalytic reactions. *Chem. Soc. Rev.* **2014**, *43*, 7624–7663. [CrossRef] [PubMed]
72. Griffiths, P.R.; De Haseth, J.A. *Fourier Transform Infrared Spectrometry*; Wiley-Interscience: New York, NY, USA, 2007; ISBN 978-0-47-119404-0.
73. Blyholder, G. Molecular Orbital View of Chemisorbed Carbon Monoxide. *J. Phys. Chem.* **1964**, *68*, 2772–2777. [CrossRef]
74. Lavalley, J.C. Infrared spectrometric studies of the surface basicity of metal oxides and zeolites using adsorbed probe molecules. *Catal. Today* **1996**, *27*, 377–401. [CrossRef]
75. Busca, G. Spectroscopic characterization of the acid properties of metal oxide catalysts. *Catal. Today* **1998**, *41*, 191–206. [CrossRef]
76. Corma, A. Inorganic Solid Acids and Their Use in Acid-Catalyzed Hydrocarbon Reactions. *Chem. Rev.* **1995**, *95*, 559–614. [CrossRef]
77. Zecchina, A.; Scarano, D.; Bordiga, S.; Ricchiardi, G.; Spoto, G.; Geobaldo, F. IR studies of CO and NO adsorbed on well characterized oxide single microcrystals. *Catal. Today* **1996**, *27*, 403–435. [CrossRef]
78. Bensitel, M.; Saur, O.; Lavalley, J.C. Use of methanol as a probe to study the adsorption sites of different MgO samples. *Mater. Chem. Phys.* **1991**, *28*, 309–320. [CrossRef]
79. Zaera, F. Infrared Absorption Spectroscopy of Adsorbed CO: New Applications in Nanocatalysis for an Old Approach. *ChemCatChem* **2012**, *4*, 1525–1533. [CrossRef]

80. Hadjiivanov, K.; Knözinger, H. Characterization of vacant coordination sites of cations on the surfaces of oxides and zeolites using infrared spectroscopy of adsorbed probe molecules. *Surf. Sci.* **2009**, *603*, 1629–1636. [CrossRef]
81. Hadjiivanov, K.I.; Vayssilov, G.N. Characterization of oxide surfaces and zeolites by carbon monoxide as an IR probe molecule. *Adv. Catal.* **2002**, *47*, 307–511. [CrossRef]
82. Hollins, P. The influence of surface defects on the infrared spectra of adsorbed species. *Surf. Sci. Rep.* **1992**, *16*, 51–94. [CrossRef]
83. Gao, F.; Wang, Y.; Goodman, D.W. CO Oxidation over AuPd(100) from Ultrahigh Vacuum to Near-Atmospheric Pressures: The Critical Role of Contiguous Pd Atoms. *J. Am. Chem. Soc.* **2009**, *131*, 5734–5735. [CrossRef] [PubMed]
84. Kim, S.; Lee, D.-W.; Lee, K.-Y. Shape-dependent catalytic activity of palladium nanoparticles for the direct synthesis of hydrogen peroxide from hydrogen and oxygen. *J. Mol. Catal. A Chem.* **2014**, *391*, 48–54. [CrossRef]
85. Kim, S.; Lee, D.-W.; Lee, K.-Y. Direct synthesis of hydrogen peroxide from hydrogen and oxygen over single-crystal cubic palladium on silica catalysts. *J. Mol. Catal. A Chem.* **2014**, *383*, 64–69. [CrossRef]
86. Ouyang, L.; Da, G.; Tian, P.; Chen, T.; Liang, G.; Xu, J.; Han, Y.-F. Insight into active sites of Pd–Au/TiO_2 catalysts in hydrogen peroxide synthesis directly from H_2 and O_2. *J. Catal.* **2014**, *311*, 129–136. [CrossRef]
87. Chul Ham, H.; Hwang, G.S.; Han, J.; Woo Nam, S.; Hoon Lim, T. On the Role of Pd Ensembles in Selective H_2O_2 Formation on PdAu Alloys. *J. Phys. Chem. C* **2009**, *113*, 12943–12945. [CrossRef]
88. Yi, C.-W.; Luo, K.; Wei, T.; Goodman, D.W. The Composition and Structure of Pd-Au Surfaces. *J. Phys. Chem. B* **2005**, *109*, 18535–18540. [CrossRef]
89. Han, Y.-F.; Zhong, Z.; Ramesh, K.; Chen, F.; Chen, L.; White, T.; Tay, Q.; Nurbaya Yaakub, S.; Wang, Z. Au Promotional Effects on the Synthesis of H_2O_2 Directly from H_2 and O_2 on Supported Pd-Au Alloy Catalysts. *J. Phys. Chem. C* **2007**, *111*, 8410–8413. [CrossRef]
90. Wilson, N.M.; Priyadarshini, P.; Kunz, S.; Flaherty, D.W. Direct synthesis of H_2O_2 on Pd and AuxPd1 clusters: Understanding the effects of alloying Pd with Au. *J. Catal.* **2018**, *357*, 163–175. [CrossRef]
91. Kunz, S.; Iglesia, E. Mechanistic Evidence for Sequential Displacement–Reduction Routes in the Synthesis of Pd–Au Clusters with Uniform Size and Clean Surfaces. *J. Phys. Chem. C* **2014**, *118*, 7468–7479. [CrossRef]
92. Edwards, J.K.; Pritchard, J.; Piccinini, M.; Shaw, G.; He, Q.; Carley, A.F.; Kiely, C.J.; Hutchings, G.J. The effect of heat treatment on the performance and structure of carbon-supported Au–Pd catalysts for the direct synthesis of hydrogen peroxide. *J. Catal.* **2012**, *292*, 227–238. [CrossRef]
93. Giorgi, J.B.; Schroeder, T.; Bäumer, M.; Freund, H.-J. Study of CO adsorption on crystalline-silica-supported palladium particles. *Surf. Sci.* **2002**, *498*, L71–L77. [CrossRef]
94. Tew, M.W.; Emerich, H.; van Bokhoven, J.A. Formation and Characterization of PdZn Alloy: A Very Selective Catalyst for Alkyne Semihydrogenation. *J. Phys. Chem. C* **2011**, *115*, 8457–8465. [CrossRef]
95. Zhang, L.; Mao, J.; Li, S.; Yin, J.; Sun, X.; Guo, X.; Song, C.; Zhou, J. Hydrogenation of levulinic acid into gamma-valerolactone over in situ reduced CuAg bimetallic catalyst: Strategy and mechanism of preventing Cu leaching. *Appl. Catal. B Environ.* **2018**, *232*, 1–10. [CrossRef]
96. Kale, M.J.; Christopher, P. Utilizing Quantitative in Situ FTIR Spectroscopy to Identify Well-Coordinated Pt Atoms as the Active Site for CO Oxidation on Al_2O_3-Supported Pt Catalysts. *ACS Catal* **2016**, *6*, 21. [CrossRef]
97. Menegazzo, F.; Burti, P.; Signoretto, M.; Manzoli, M.; Vankova, S.; Boccuzzi, F.; Pinna, F.; Strukul, G. Effect of the addition of Au in zirconia and ceria supported Pd catalysts for the direct synthesis of hydrogen peroxide. *J. Catal.* **2008**, *257*, 369–381. [CrossRef]
98. Groppo, M.E.; Bertarione, S.; Rotunno, F.; Agostini, G.; Scarano, D.; Pellegrini, R.; Leofanti, G.; Zecchina, A.; Lamberti, C. Role of the Support in Determining the Vibrational Properties of Carbonyls Formed on Pd Supported on SiO. *J. Phys. Chem. C* **2007**, *111*, 7021–7028. [CrossRef]
99. Roques, J.; Lacaze-Dufaure, C.; Mijoule, C. Dissociative Adsorption of Hydrogen and Oxygen on Palladium Clusters: A Comparison with the (111) Infinite Surface. *J. Chem. Theory Comput.* **2007**, *3*, 878–884. [CrossRef] [PubMed]

100. Wei, T.; Wang, J.; Goodman, D.W. Characterization and Chemical Properties of Pd−Au Alloy Surfaces. *J. Phys. Chem. C* **2007**, *111*, 8781–8788. [CrossRef]
101. Schalow, T.; Brandt, B.; Starr, D.E.; Laurin, M.; Shaikhutdinov, S.K.; Schauermann, S.; Libuda, J.; Freund, H.-J. Particle size dependent adsorption and reaction kinetics on reduced and partially oxidized Pd nanoparticles. *Phys. Chem. Chem. Phys.* **2007**, *9*, 1347–1361. [CrossRef] [PubMed]
102. Wolter, K.; Seiferth, O.; Libuda, J.; Kuhlenbeck, H.; Bäumer, M.; Freund, H.-J. IR spectroscopy of a Pd-carbonyl surface compound. *Chem. Phys. Lett.* **1997**, *277*, 513–520. [CrossRef]
103. Abate, S.; Centi, G.; Melada, S.; Perathoner, S.; Pinna, F.; Strukul, G. Preparation, performances and reaction mechanism for the synthesis of H_2O_2 from H_2 and O_2 based on palladium membranes. *Catal. Today* **2005**, *104*, 323–328. [CrossRef]
104. Edwards, J.K.; Solsona, B.; Landon, P.; Carley, A.F.; Herzing, A.; Watanabe, M.; Kiely, C.J.; Hutchings, G.J. Direct synthesis of hydrogen peroxide from H_2 and O_2 using Au–Pd/Fe_2O_3 catalysts. *J. Mater. Chem.* **2005**, *15*, 4595. [CrossRef]
105. Enache, D.I.; Edwards, J.K.; Landon, P.; Solsona-Espriu, B.; Carley, A.F.; Herzing, A.A.; Watanabe, M.; Kiely, C.J.; Knight, D.W.; Hutchings, G.J. Solvent-free oxidation of primary alcohols to aldehydes using Au-Pd/TiO_2 catalysts. *Science* **2006**, *311*, 362–365. [CrossRef]
106. Herzing, A.A.; Carley, A.F.; Edwards, J.K.; Hutchings, G.J.; Kiely, C.J. Microstructural Development and Catalytic Performance of Au−Pd Nanoparticles on Al_2O_3 Supports: The Effect of Heat Treatment Temperature and Atmosphere. *Chem. Mater.* **2008**, *20*, 1492–1501. [CrossRef]
107. Sales, E.A.; Jove, J.; de Jesus Mendes, M.; Bozon-Verduraz, F. Palladium, Palladium–Tin, and Palladium–Silver Catalysts in the Selective Hydrogenation of Hexadienes: TPR, Mössbauer, and Infrared Studies of Adsorbed CO. *J. Catal.* **2000**, *195*, 88–95. [CrossRef]
108. Schalow, T.; Brandt, B.; Laurin, M.; Schauermann, S.; Guimond, S.; Kuhlenbeck, H.; Libuda, J.; Freund, H.-J. Formation of interface and surface oxides on supported Pd nanoparticles. *Surf. Sci.* **2006**, *600*, 2528–2542. [CrossRef]
109. Hinojosa, J.A., Jr.; Kan, H.H.; Weaver, J.F. Molecular Chemisorption of O_2 on a PdO(101) Thin Film on Pd(111). *J. Phys. Chem. C* **2008**, *112*, 8324–8331. [CrossRef]
110. Ozensoy, E.; Wayne Goodman, D. Vibrational spectroscopic studies on CO adsorption, NO adsorption CO + NO reaction on Pd model catalysts. *Phys. Chem. Chem. Phys.* **2004**, *6*, 3765–3778. [CrossRef]
111. Yuan, D.; Gong, X.; Wu, R. Peculiar distribution of Pd on Au nanoclusters: First-principles studies. *Phys. Rev. B* **2008**, *78*, 035441. [CrossRef]
112. Lee, S.; Jeong, H.; Chung, Y.-M. Direct synthesis of hydrogen peroxide over Pd/C catalyst prepared by selective adsorption deposition method. *J. Catal.* **2018**, *365*, 125–137. [CrossRef]
113. Fanning, P.E.; Vannice, M.A. A DRIFTS study of the formation of surface groups on carbon by oxidation. *Carbon* **1993**, *31*, 721–730. [CrossRef]
114. Figueiredo, J.; Pereira, M.F.; Freitas, M.M.; Órfão, J.J. Modification of the surface chemistry of activated carbons. *Carbon* **1999**, *37*, 1379–1389. [CrossRef]
115. Reddy, C.R.; Bhat, Y.S.; Nagendrappa, G.; Jai Prakash, B.S. Brønsted and Lewis acidity of modified montmorillonite clay catalysts determined by FT-IR spectroscopy. *Catal. Today* **2009**, *141*, 157–160. [CrossRef]
116. Jin, F.; Li, Y. A FTIR and TPD examination of the distributive properties of acid sites on ZSM-5 zeolite with pyridine as a probe molecule. *Catal. Today* **2009**, *145*, 101–107. [CrossRef]
117. Chakraborty, B.; Viswanathan, B. Surface acidity of MCM-41 by in situ IR studies of pyridine adsorption. *Catal. Today* **1999**, *49*, 253–260. [CrossRef]
118. Emeis, C.A. Determination of Integrated Molar Extinction Coefficients for Infrared Absorption Bands of Pyridine Adsorbed on Solid Acid Catalysts. *J. Catal.* **1993**, *141*, 347–354. [CrossRef]
119. Glazneva, T.S.; Kotsarenko, N.S.; Paukshtis, E.A. Surface acidity and basicity of oxide catalysts: From aqueous suspensions to in situ measurements. *Kinet. Catal.* **2008**, *49*, 859–867. [CrossRef]
120. Sen, S.; Wusirika, R.R.; Youngman, R.E. High temperature thermal expansion behavior of H[Al]ZSM-5 zeolites: The role of Brønsted sites. *Microporous Mesoporous Mater.* **2006**, *87*, 217–223. [CrossRef]
121. Essayem, N.; Holmqvist, A.; Gayraud, P.; Vedrine, J.; Ben Taarit, Y. In Situ FTIR Studies of the Protonic Sites of $H_3PW_{12}O_{40}$ and Its Acidic Cesium Salts MxH3−xPW12O40. *J. Catal.* **2001**, *197*, 273–280. [CrossRef]

122. Gemo, N.; Biasi, P.; Canu, P.; Menegazzo, F.; Pinna, F.; Samikannu, A.; Kordás, K.; Salmi, T.O.; Mikkola, J.-P. Reactivity Aspects of SBA15-Based Doped Supported Catalysts: H_2O_2 Direct Synthesis and Disproportionation Reactions. *Top. Catal.* **2013**, *56*, 540–549. [CrossRef]
123. Gibson, E.K.; Beale, A.M.; Richard, C.; Catlow, A.; Chutia, A.; Gianolio, D.; Gould, A.; Kroner, A.; Mohammed, K.M.H.; Perdjon, M.; et al. Restructuring of AuPd Nanoparticles Studied by a Combined XAFS/DRIFTS Approach. *Chem. Mater.* **2015**, *27*, 3714–3720. [CrossRef]